Virology 489 (2016) 252–268

Contents lists available at ScienceDirect

Virology

journal homepage: www.elsevier.com/locate/yviro

Suppression of type I interferon production by porcine epidemic diarrhea virus and degradation of CREB-binding protein by nsp1

Qingzhan Zhang [1], Kaichuang Shi [1,2], Dongwan Yoo *

Department of Pathobiology, University of Illinois at Urbana–Champaign, Urbana 61802, IL, USA

ARTICLE INFO

Article history:
Received 3 October 2015
Returned to author for revisions
20 October 2015
Accepted 19 December 2015
Available online 14 January 2016

Keywords:
CREB-binding protein
Porcine epidemic diarrhea virus
Coronavirus
Interferon regulation
CBP
Nsp1
Innate immune signaling

ABSTRACT

Type I interferons (IFN-α/β) are the major components of the innate immune response of hosts, and in turn many viruses have evolved to modulate the host response during infection. We found that the IFN-β production was significantly suppressed during PEDV infection in cells. To identify viral IFN antagonists and to study their suppressive function, viral coding sequences for the entire structural and nonstructural proteins were cloned and expressed. Of 16 PEDV nonstructural proteins (nsps), nsp1, nsp3, nsp7, nsp14, nsp15 and nsp16 were found to inhibit the IFN-β and IRF3 promoter activities. The sole accessory protein ORF3, structure protein envelope (E), membrane (M), and nucleocapsid (N) protein were also shown to inhibit such activities. PEDV nsp1 did not interfere the IRF3 phosphorylation and nuclear translocation but interrupted the enhanceosome assembly of IRF3 and CREB-binding protein (CBP) by degrading CBP. A further study showed that the CBP degradation by nsp1 was proteasome-dependent. Our data demonstrate that PEDV modulates the host innate immune responses by degrading CBP and suppressing ISGs expression.

Introduction

Porcine epidemic diarrhea (PED) is a highly contagious acute enteric disease characterized by vomiting, watery diarrhea, and severe dehydration of up to 80–100% mortality in suckling piglets (Song and Park, 2012; Sun et al., 2012a; Debouck and Pensaert, 1980; Junwei et al., 2006). PED was first reported in England in feeder and fattening pigs during 1970s (Wood, 1977), and re-emerged in Asia since 2010 with greater virulence and economic losses (Chen et al., 2013; Li et al., 2012; Puranaveja et al., 2009; Yang et al., 2013). In the US, PEDV appeared for the first time in 2013 and severely affected most pig-producing states (Chen et al., 2014; Marthaler et al., 2013; Mole, 2013; Stevenson et al., 2013). The causative agent is porcine epidemic diarrhea virus (PEDV), which belongs to the *Alphacoronavirus* genus in the family *Coronaviridae* (http://ictvonline.org/virustaxonomy.asp). PEDV is an enveloped virus with a single-stranded positive-sense RNA genome of approximately 28 kb in length with the 5′-cap and the 3′-polyadenylated tail. The PEDV genome is arranged with ORF1a, ORF1b, S, ORF3, E, M, N, in order with both termini flanking with the 5′- and 3′-untranslated regions (UTRs) (Duarte et al., 1993). ORF1a codes for the large polyprotein PP1a, while ORF1b is always expressed as a fusion protein PP1a/b with PP1a through a ribosomal frameshifting. PP1a and PP1a/b are further processed to 16 nonstructural proteins, nsp1 through nsp16. ORF3 codes for an accessory protein which is likely an additional nonstructural protein, whereas S, E, M and N genes code for four structural proteins (Song and Park, 2012).

During viral infection, the sensing of foreign nucleic acids in the cytosol leads to the activation of an innate immune response to produce type I interferons (IFN-α/β) and establishes an antiviral state. The type I IFNs and IFN-mediated response provide a first line of defense against viral infection. The host innate immune system deploys the pattern-recognition receptors (PRRs) to sense and respond to the pathogen-associated molecular patterns (PAMPs) of virus (Kawai and Akira, 2011). This recognition triggers the activation of retinoic acid-inducible gene I (RIG-I) or melanoma differentiation gene 5 (MDA5), which further binds to the mitochondrial adapter protein MAVS/IPS-1 and recruits TNF receptor-associated factor 3/6 (TRAF3 and TRAF6). TRAF3 activates IκB kinase (IKK)-related kinases such as TANK-binding kinase 1 (TBK1) and IKKε for phosphorylation of interferon regulatory factors 3 and 7 (IRF3/IRF7) and type I IFN production (Fitzgerald et al., 2003; Sharma et al., 2003). TRAF6 leads to TANK1 activation, followed by NF-kB activation and cytokine production (Rajsbaum and Garcia-Sastre, 2013). Upon TBK1 activation, phosphorylated IRF3 undergoes homodimerization and unveils the nuclear localization signal leading to the nuclear translocation, where it forms a

* Corresponding author. Tel.: +1 217 244 9120.
E-mail address: dyoo@illinois.edu (D. Yoo).
[1] Equal contribution to the study.
[2] Current address: Guangxi Center for Animal Disease Control and Prevention, Nanning, Guangxi, China.

http://dx.doi.org/10.1016/j.virol.2015.12.010
0042-6822/

complex with the transcription co-activator CREB (cAMP responsive element binding)-binding protein (CBP)/p300 (Dragan et al., 2007; Lin et al., 1998; Panne et al., 2007). The IRF3-CBP/p300 complex further binds to the positive regulatory domain (PRD) I–IV regions of the IFN-β promoter to assemble the enhanceosome together with NF-κB and other factors to turn on the transcription of type I IFN genes (Honda and Taniguchi, 2006). The IRF3–CBP/p300 interaction is crucial for IFN transcription. Following production and secretion, IFN molecules bind to the cell surface receptors and trigger the activation of Janus kinase–signal transducers and activators of transcription (JAK–STAT) signaling cascade. Phosphorylated STAT1 and STAT2 associate to form a heterodimer, which in turn recruits the IFN-regulatory factor 9 (IRF9) to form the IFN-stimulated gene factor 3 (ISGF3). ISGF3 translocates to the nucleus and induces genes regulated by IFN-stimulated response elements (ISRE), resulting in expression of hundreds of antiviral genes and establishment of an antiviral state (Stark and Darnell, 2012).

In turn, many viruses have evolved to counteract the host innate immune defense and such viral functions are often redundant. For *nidoviruses*, eleven and six viral proteins have been described as IFN antagonists for severe acute respiratory syndrome

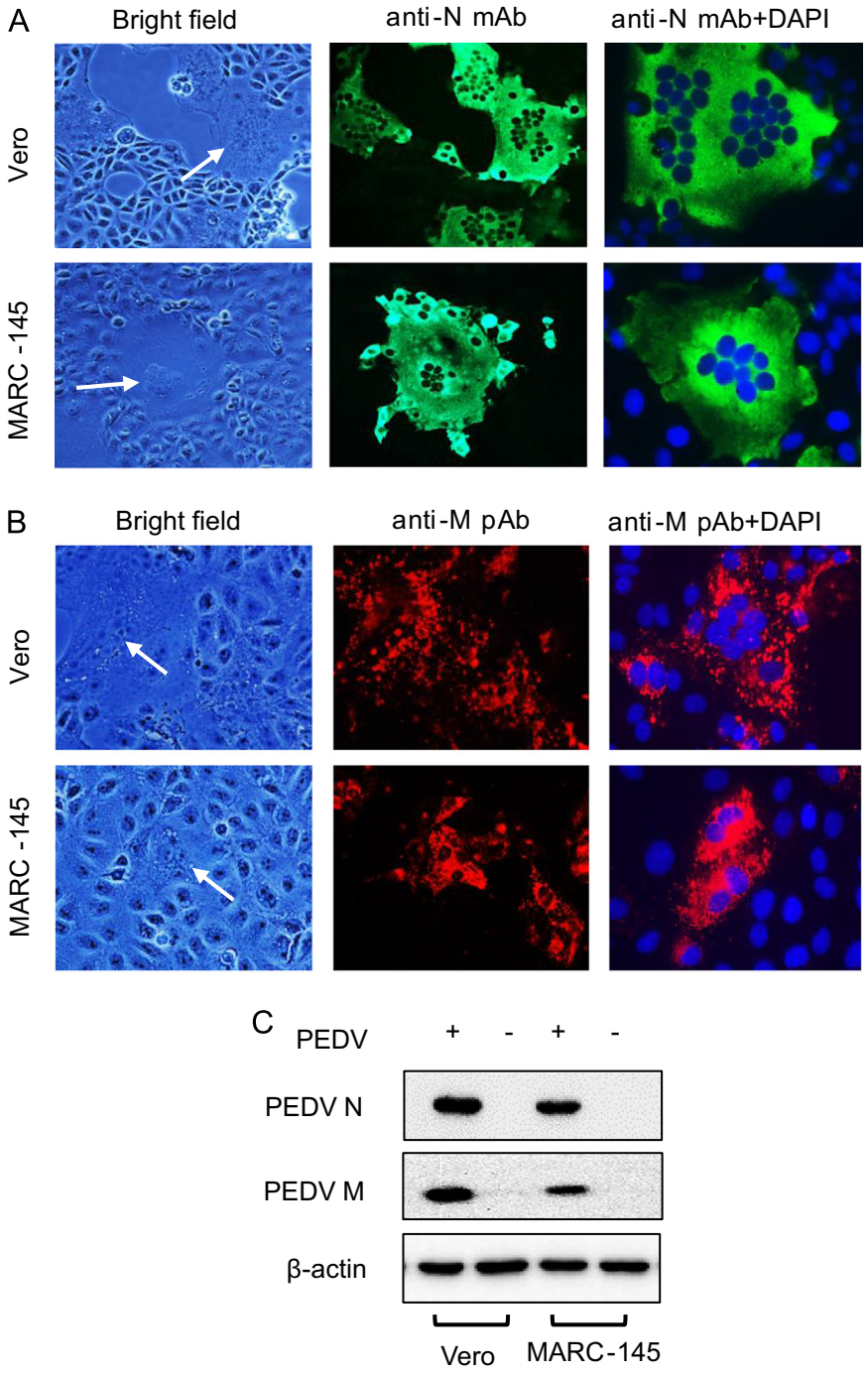

Fig. 1. *PEDV infection in Vero and MARC-145 cells.* (A and B) Immunofluorescence showing the expression of nucleocapsid (N, green) and membrane (M, red) proteins in PEDV-infected cells. Vero and MARC-145 cells were infected with PEDV at an MOI of 0.1. Cells were fixed with 4% paraformaldehyde in PBS and stained with mouse anti-N monoclonal antibody (mAb) or rabbit anti-M polyclonal antibody (pAb). Arrows show multi-nucleated cells by fusion. (C) Detection of the N and M proteins in PEDV-infected cells. Cell lysates were prepared at 24 h post-infection, and Western blots were conducted using antibodies against N and M proteins.

coronavirus (SARS-CoV) and porcine reproductive and respiratory syndrome virus (PRRSV), respectively (Huang et al., 2014; Kindler and Thiel, 2014; Shi et al., 2014; Sun et al., 2012b; Totura and Baric, 2012). For *Betacoronaviruses,* nsp1 has been reported as a multifunctional viral antagonist for innate immune response (Huang et al., 2011b; Narayanan et al., 2008; Wang et al., 2010). For PEDV, the viral modulation of innate immune signaling is poorly understood. PEDV infects Vero cells, but these cells are type I IFN-deficient due to a chromosomal deletion (Desmyter et al., 1968). In the present study, we identified MARC-145 cells as a suitable line of cells for PEDV infection and for study of innate immune modulation. We showed that PEDV suppressed the type I interferon production and ISGs expression in these cells, and identified nsp1, nsp3, nsp7, nsp14, nsp15, nsp16, E, M, N and ORF3 as the viral IFN antagonists. We showed that PEDV nsp1 caused the CBP degradation by the proteasome-dependent pathway. The CBP degradation is a novel mechanism of coronavirus nsp1 for IFN suppression and our study provides a new insight into the immune modulation and evasion strategy of PEDV.

Results

Infection of PEDV in Vero and MARC-145 cells

PEDV replicates in the cytoplasm of villous epithelial cells of the small and large intestines (Debouck and Pensaert, 1980; Sueyoshi et al., 1995). The viral antigen is also detectable in the macrophages that infiltrated the lamina propria (Lee et al., 2000). Histological studies showed that PEDV replicates in the porcine respiratory tract *in vivo* and transformed alveolar macrophages (3D4) *in vitro* (Park and Shin, 2014). Vero cells are widely used for PEDV for diagnosis, virus isolation, and research, but these cells are type I IFN-deficient due to the chromosomal deletion (Desmyter et al., 1968). To study a possible regulation of innate immune signaling by PEDV, various cell lines were examined for susceptibility. Cells were infected with PEDV at an MOI of 0.1 in various trypsin concentrations and CPE was examined daily for up to 5 days. In Vero and MARC-145 cells, apparent CPE of multinucleation was observed by 24 h post-infection (Fig. 1A and B, left panel). Trypsin activates the cleavage of S protein and induces membrane fusion to trigger infection (Park et al., 2011; Wicht et al., 2014). PEDV infection was characterized by syncytia formation (Hofmann and Wyler, 1988) and infection foci were visualized by anti-PEDV M and N antibodies, indicating the susceptibility of both cell types for PEDV infection (Fig. 1A and B, middle and right panel). The viral proteins were detected using specific antibodies by western blot and the specific bands were corresponding to the M and N proteins, further confirming the productive infection of these cells by PEDV (Fig. 1C). The optimal trypsin concentration for PEDV propagation was 5 μg/ml and 2 μg/ml for Vero and MARC-145 cells, respectively. MARC-145 cells have been used to study type I IFN signaling of porcine arterivirus (Kim et al., 2010; Overend et al., 2007; Patel et al., 2010), and thus infection of these cells

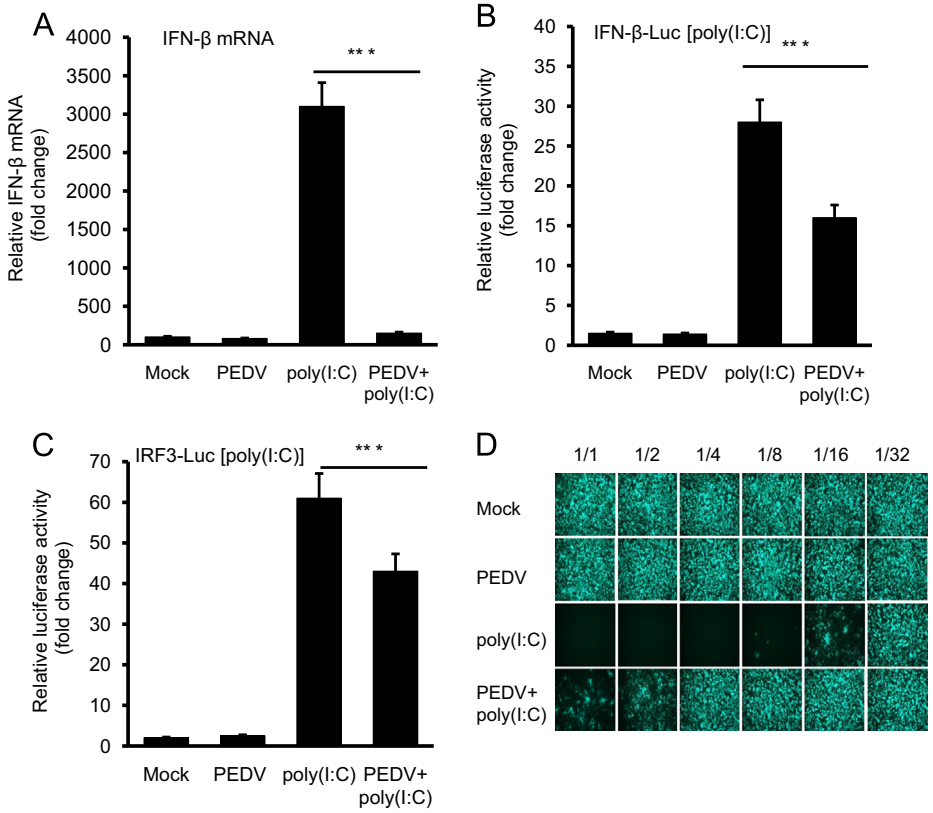

Fig. 2. *Suppression of IFN-β production by PEDV.* (A) Inhibition of IFN-β gene transcription in virus-infected cells. MARC-145 cells were infected with PEDV at an MOI of 1 for 12 h in 12-well plates. Cells were transfected with poly(I:C) (0.5 μg/well) for 12 h, and qRT-PCR was conducted for IFN-β mRNA. Relative quantitation values for IFN-β mRNA are presented. (B and C), Regulation of IFN-β and IRF3 activities by PEDV. MARC-145 cells were co-transfected with pIFN-β-Luc (B), or pIRF3-Luc (C) along with pRL-TK in 12-well plates for 6 h followed by PEDV infection at an MOI of 1 for 12 h. Cells were then stimulated with poly(I:C) for 12 h, and cell lysates were prepared for dual-luciferase reporter assay. Results from three independent experiments were expressed as mean relative luciferase with standard deviation. Each experiment was carried out in triplicate. Asterisks indicate statistical significance calculated by the Student's *t* test. $^{*}P < 0.05$, $^{**}P < 0.01$, $^{***}P < 0.001$. (D) VSV–GFP bioassay for IFN production. MARC-145 cells were infected with PEDV in 6-well plates at an MOI of 1 for 12 h and stimulated with poly(I:C) for 12 h. Cell culture supernatants were collected and UV-irradiated for 30 min. Fresh MARC-145 cells were grown in 96-well plates and incubated with supernatants of 2-fold serial dilutions of up to 1:32. After 24 h of incubation, cells were infected with VSV–GFP at an MOI of 0.1 for 16 h. GFP expression was assessed by fluorescent microscopy. Each dilution was tested in triplicate.

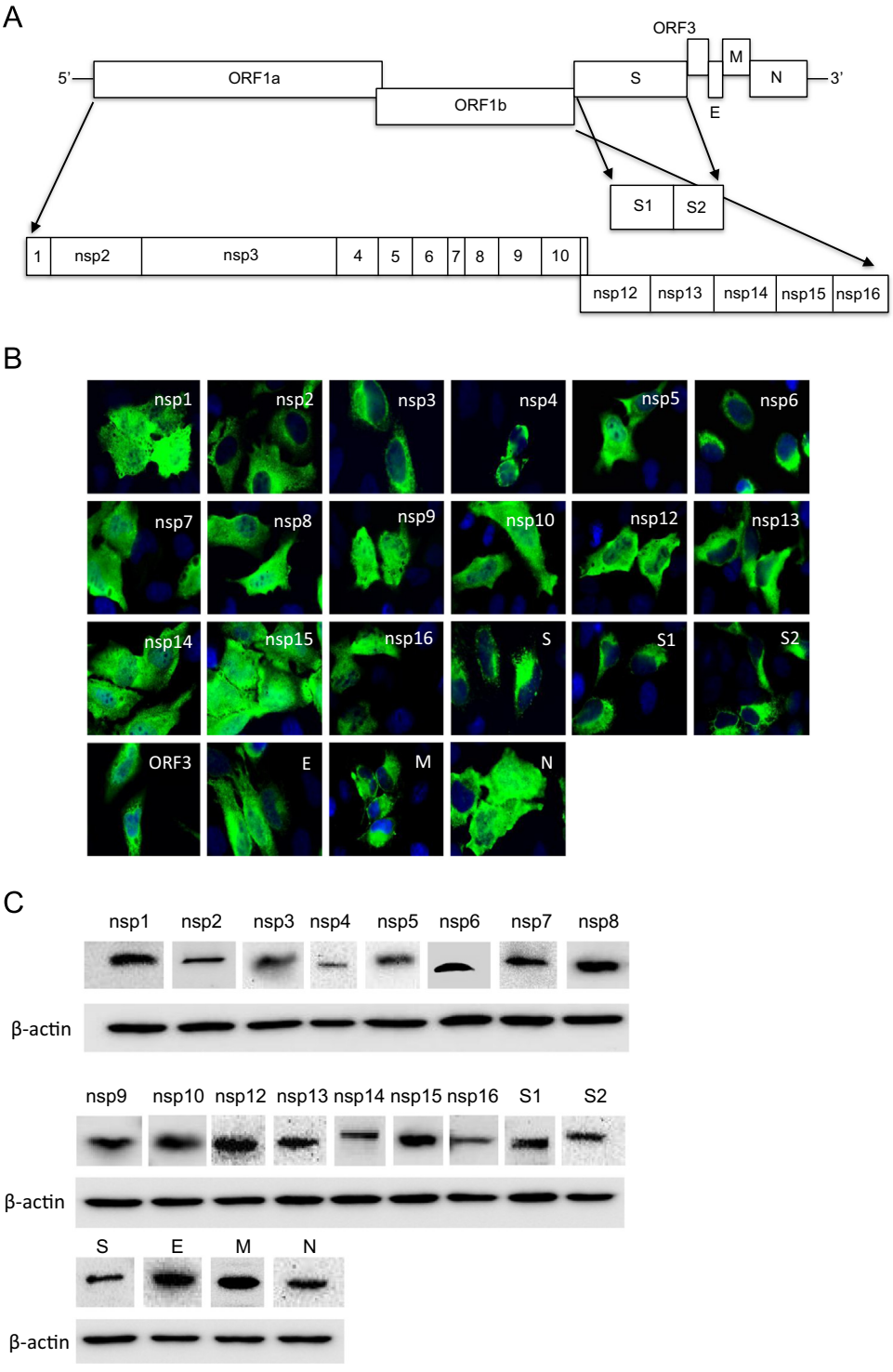

Fig. 3. *Cloning of PEDV genes and identification of viral proteins antagonizing type I IFN cascade*. (A) Genome organization of PEDV. The PEDV genome is organized as 5′ UTR-ORF1a-ORF1b-S(S1+S2)-ORF3-E-M-N-3′UTR in order. Sixteen nonstructural proteins encoded in ORF1a and ORF1b are depicted. (B and C) Confirmation of cloned gene expression. One μg of each of the cloned genes was transfected to HeLa cells in 12-well plates, and protein expression was determined by immunofluorescence (B) and Western blot (C) for each gene using anti-FLAG antibody. (D and E) Regulation of poly(I:C)-induced IFN-β promoter activity by individual PEDV proteins. HeLa cells were seeded in 12-well plates and co-transfected with pIFN-β-Luc along with individual PEDV genes and pRL-TK at a ratio of 1:1:0.1. Since the expression levels of nsp3 and nsp16 were low, three-times more plasmids were transfected for these genes to ensure the comparable level of protein expression. PRRSV nsp1α (P-nsp1α) is a known type I IFN suppressor, and the IFN-suppression of its mutant P-nsp1α(m) was lost. Both constructs were included as controls. At 24 h post-transfection, cells were stimulated with poly (I:C) (0.5 μg/ml) for 12 h and the luciferase activities were measured. The reporter experiments were repeated three times, each time in triplicate. Asterisks indicate the statistical significance. Statistical analysis was performed by Student's *t* test using GST as a control. $^{*}P<0.05$, $^{**}P<0.01$ and $^{***}P<0.001$. (F) VSV–GFP bioassay. The cell culture supernatants for IFN-β promoter luciferase assays were collected and diluted serially by 2-folds up to 1:64. Fresh MARC-145 cells were grown in 96-well plates and incubated with each dilution of supernatants for 24 h, and then infected with VSV–GFP at an MOI of 0.1 for 16 h. VSV replication was measured by monitoring the fluorescence by GFP expression using fluorescent microscopy. Data were presented as $\log_2$ sample dilution folds. (G) Inhibition of IRF3 promoter activation by PEDV proteins. The IFN antagonists were further examined for IRF3 activities by luciferase reporter assays. Statistical analysis was performed by Student's *t* test using GST as a control. $^{*}P<0.05$, $^{**}P<0.01$ and $^{***}P<0.001$.

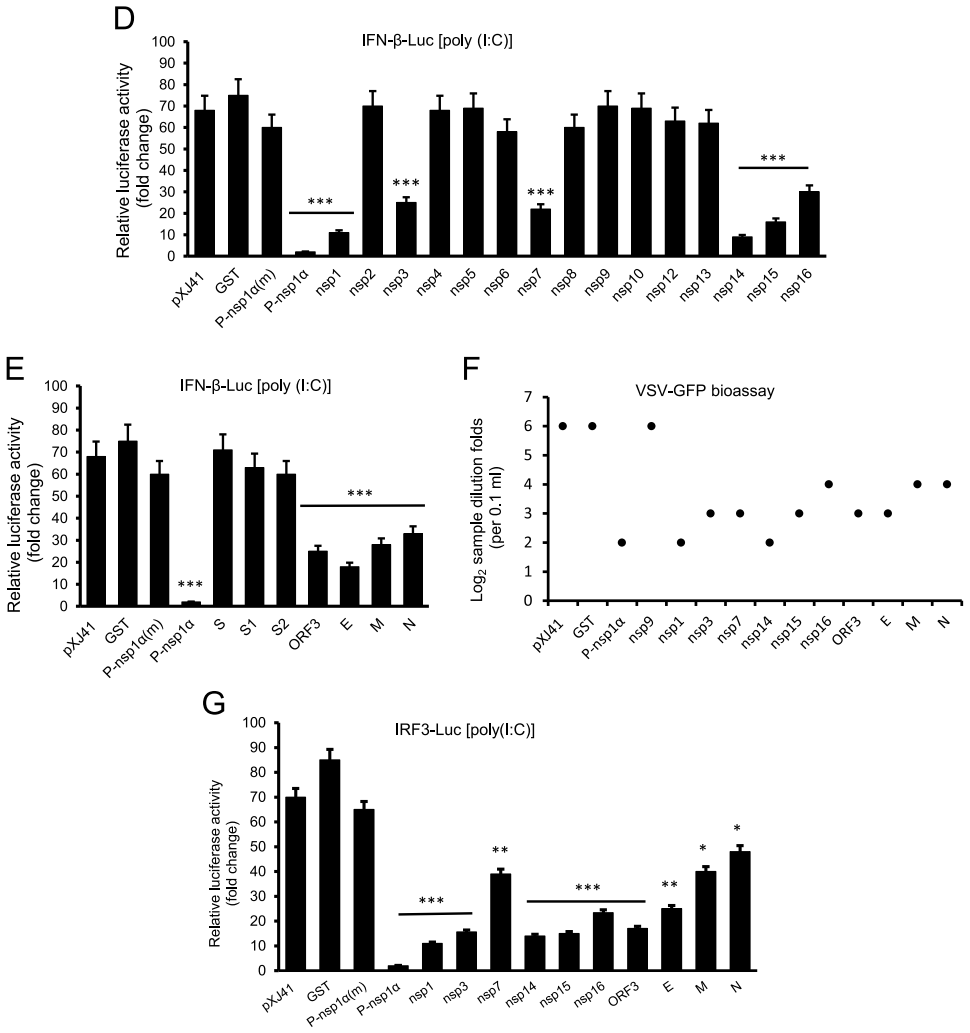

Fig. 3. (*continued*)

by PEDV allowed us to study IFN modulation and signaling cascade.

Suppression of IFN-β production in PEDV-infected cells

To determine whether PEDV infection antagonized the type I IFN response, IFN-β mRNA was determined in virus-infected cells. MARC-145 cells were infected with PEDV and stimulated with poly (I:C) followed by qRT-PCR for IFN-β mRNA using total RNA. As shown in Fig. 2A, PEDV infection did not induce the level of IFN-β mRNA expression whereas poly(I:C) alone induced the IFN-β gene expression effectively, indicating the suppression of IFN-β response by PEDV. To further evaluate the IFN-β response in PEDV-infected cells, a dual luciferase assay was performed. The results showed the suppression of IFN-β promoter activity in PEDV-infected cells upon poly(I:C) stimulation (Fig. 2B), demonstrating the modulation of IFN production by PEDV infection. IRF3 was additionally examined for its role for PEDV-mediated IFN-β suppression. The IRF3 promoter activity was found to be inhibited (Fig. 2C). The suppression of IFN-β production was confirmed by bioassay using VSV–GFP. VSV is sensitive to type I IFN treatment and thus commonly used for IFN bioassays. Culture supernatants were collected from PEDV-infected cells and were UV-irradiated, followed by incubation with MARC-145 cells and infection with VSV–GFP. VSV grew normally (Fig. 2D), whereas it did not grow with supernatants collected from poly(I:C)-treated cells for up to 1:8 dilution. VSV–GFP also grew normally with supernatants from both PEDV-infected cells with or without poly(I:C) stimulation, confirming the suppression of type I IFN production by PEDV.

Identification of viral IFN antagonists

The viral IFN antagonism is often redundant, and at least 11 viral proteins have been identified as IFN antagonists for SARS-CoV (Kindler and Thiel, 2014; Shi et al., 2014; Totura and Baric, 2012). To identify such proteins for PEDV, we cloned PEDV genes representing nsps 1 through 16, and structural genes for S, E, M, and N including the ORF3 accessory protein gene (Fig. 3A). Among these, nsp11 is a small oligopeptide generated from PP1a when ribosomal frameshifting does not occur and so was not included in this study. Each gene was inserted into the pXJ41 expression vector with the FLAG tag at either N- or C-terminus, and examined for IFN suppression. The protein expression of cloned genes was examined by immunofluorescence (Fig. 3B) and western blot (Fig. 3C) using anti-FLAG antibody. All genes were expressed as anticipated. HeLa cells were then co-transfected with an individual gene along with pIFN-β-Luc and pRL-TK, and reporter assays were conducted. PRRSV nsp1α (P-nsp1α) is known as an IFN-β suppressor, and its cystine mutant P-nsp1α(m) (C28S) is an IFN suppression revertant (Han et al., 2013; Song et al., 2010), and so they were included as positive and negative controls, respectively. Poly(I:C) upregulated the IFN-β transcription in cells expressing pXJ41, GST, and P-nsp1α

(m), while P-nsp1α suppressed the IFN-β promoter activity as expected (Fig. 3D and E). Of the nsps, nsp1, nsp3, nsp7, nsp14, nsp15 and nsp16 were shown to down-regulate the IFN-β activity (Fig. 3D). For structural proteins, E, M, and N were found to suppress the IFN induction (Fig. 3E), and ORF3 was additionally identified as an IFN suppressive protein (Fig. 3E). The findings from the reporter assays were validated by VSV–GFP bioassays. The dilution corresponding to 50% of cells exhibiting GFP expression was determined as the end-point inhibition. For pXJ41, GST, and nsp9, GFP expression was evident and their end-point inhibitions were determined as 1:64 (Fig. 3F). In contrast, the viral proteins identified as the luciferase suppressors showed an apparent inhibition of VSV–GFP replication and their end-points were determined to be 1:4 to 1:16 (Fig. 3F). These titers represent 4- to 16-fold lower than those of controls. Taken together, these data demonstrate that PEDV has the ability for IFN suppression, and nsp1, nsp3, nsp7, nsp14, nsp15, nsp16, ORF3, E, M and N are the viral IFN antagonists.

To determine the target for IFN inhibition, the IRF3 pathway was examined for individual viral proteins using the IRF3 luciferase reporter constructs. Upon stimulation, the IRF3-dependent luciferase expression was reduced by nsp1, nsp3, nsp7, nsp14, nsp15, nsp16, ORF3, E, M, and N, comparing to those of pXJ41 and GST (Fig. 3G). This suggests that the IRF3 signaling pathway was interfered by these viral proteins for the suppression of the IFN-β production.

PEDV nsp1 antagonism is a nuclear event

SARS-CoV is a *betacoronavirus* and its nsp1 triggers inhibition of type I IFN induction and downstream signaling, host mRNA decay and cleavage, and inhibition of protein translation (Huang et al., 2011b; Lokugamage et al., 2012; Narayanan et al., 2008; Tanaka et al., 2012). Transmissible gastroenteritis virus (TGEV) is an *alphacoronavirus* and its nsp1 inhibits host protein expression (Huang et al., 2011a). Nsp1 of *alphacoronavirus* and *betacoronavirus* lacks the overall sequence similarity (Narayanan et al., 2015), and thus *alphacoronavirus* nsp1 may have a distinct basis for its biological function. Since nsp1 appeared the most potent suppressor in our study on PEDV, nsp1 was chosen to study the molecular basis for the IFN suppression. The subcellular localization was first examined by confocal microscopy in transiently expressing cells. The nsp1 distribution was evident in the both nucleus and cytoplasm (Fig. 4A), which is consistent with TGEV nsp1 (Narayanan et al., 2015). Co-expression of nsp1 with either the endoplasmic reticulum or mitochondrial marker showed the site for cytoplasmic nsp1 in the endoplasmic reticulum (Fig. 4B). Quantitative RT-PCR was conducted to evaluate IFN-β suppression in nsp1-gene transfected cells. The expression of nsp1 significantly suppressed the IFN-β mRNA transcription (Fig. 5A), further validating the nsp1 antagonism against IFN-β production. Subsequently, the IFN-mediated antiviral gene expression was examined for ISG15 and ISG56 by qRT-PCR. PEDV nsp1 reduced the poly(I:C)-stimulated mRNA levels of both ISG15 (Fig. 5B) and ISG56 (Fig. 5C), indicating the suppression of IFN signaling by nsp1. The suppression of IFN-β, IRF3, and NF-κB activations raises a possibility that nsp1 may target a component of the RIG-I like receptor (RLR) signaling pathway. To examine this premise, nsp1 was co-expressed with one of the main components in the RLR signaling pathway, and IFN luciferase activities were determined at 24 h post-transfection. The over-expression of IPS-1, or IRF3 led to the robust activation of the IFN-β promoter as anticipated, whereas the activation was significantly inhibited by nsp1 (Fig. 6A and B). Collectively, it suggests that nsp1 targets the RLR pathway downstream of the IRF3 activation.

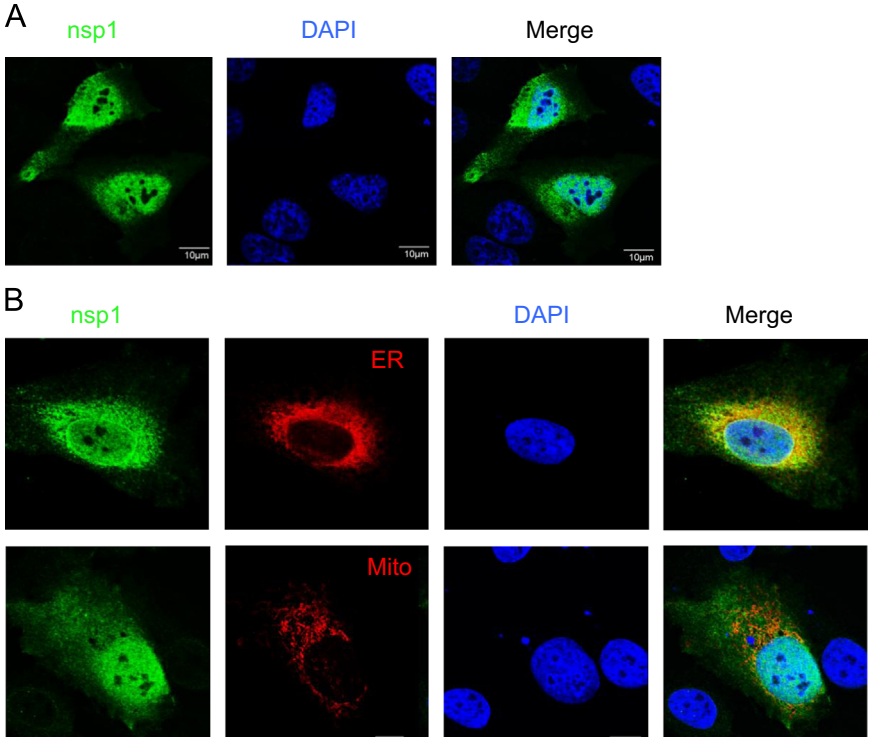

Fig. 4. *Subcellular localization of PEDV nsp1*. HeLa cells were seeded on slides in 6-well plates and transfected with PEDV nsp1 gene (A), or co-transfected with nsp1 and pDsRed2-ER or pDsRed2-Mito (B). At 24 h post-transfection, cells were fixed and permeabilized with Triton X-100. Cells were then incubated with rat anti-FLAG mAb for 1 h, followed by Alexa Fluor 488-conjugated goat anti-mouse (green) secondary antibody to visualize nsp1. The ER and mitochondrial proteins were fused with the ER and mitochondria targeting sequence (Clontech) and so directly visualized (red). Nuclei (blue) were stained with DAPI. Images were collected using a Zeiss LSM-510 META confocal laser-scanning microscope and processed with the LSM image browser (Zeiss).

IRF3 is a resident protein in the cytoplasm. When stimulated, it is phosphorylated and homodimerized, leading to the translocation to the nucleus (Dragan et al., 2007). To determine whether PEDV nsp1 targeted the IRF3-dependent pathway, the IRF3 phosphorylation was first examined. nsp1-gene transfected cells were stimulated with poly(I:C), and the IRF3 phosphorylation was examined by western blot. As anticipated, the poly(I:C) stimulation led to IRF3 phosphorylation in pXJ41-transfected cells, and similarly, in nsp1-expressing cells, the IRF3 phosphorylation was evident and comparable to that of control (Fig. 7A, top panel, lane 4), suggesting that PEDV nsp1 exerts its suppression downstream of the IRF3 phosphorylation. Thus, the nuclear translocation of IRF3 was next examined. PRRSV nsp1α is known not to block the IRF3 nuclear localization, and so was used as a control in this study. Endogenous IRF3 was normally diffused and distributed in the cytoplasm, but translocated to the nucleus when stimulated by poly(I:C) (Fig. 7B, second panel). Similarly to PRRSV nsp1α-expressing cells (Fig. 7B, fourth panel), IRF3 also localized normally in the nucleus after stimulation in PEDV nsp1-expressing cells (Fig. 7B, bottom panel), suggesting that the IFN suppression by PEDV nsp1 may be a nuclear event. The IRF3 nuclear translocation in nsp1-expressing cells was further confirmed by cell fractionation and western blot analyses. While IRF3 was phosphorylated and localized in the nucleus after stimulation, PEDV nsp1 did not inhibit the IRF3 phosphorylation and nuclear translocation (Fig. 7C), further indicating that the nsp1-mediated IFN suppression was a nuclear event.

Interruption of IRF3 and CBP association by nsp1

After nuclear translocation, an IRF3 dimer associates with the CREB-binding protein (CBP). This complex then binds to the PRD I–III

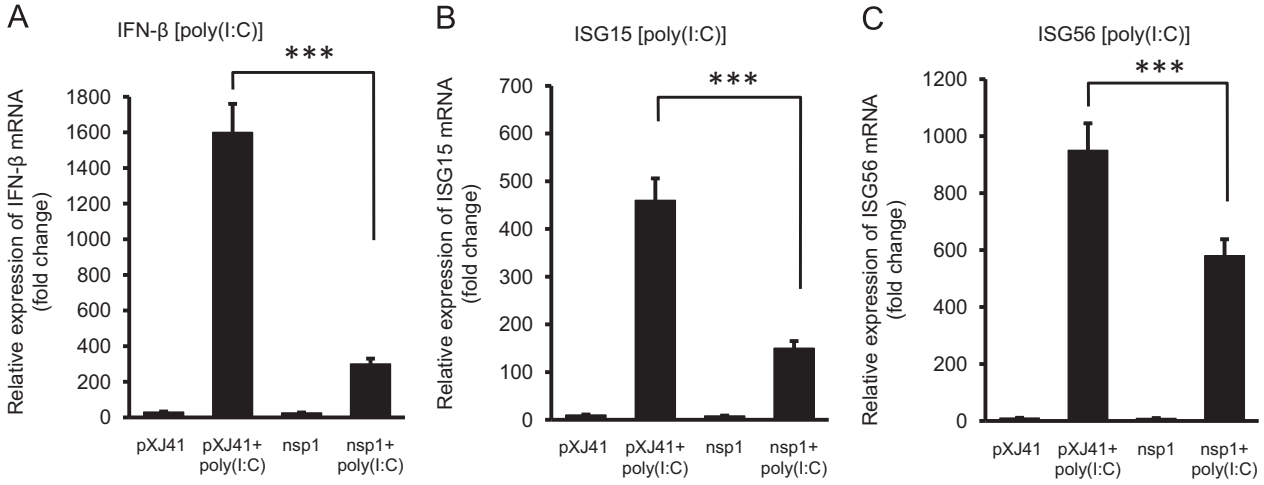

Fig. 5. *Inhibition of IFN-β and ISG expression by nsp1.* HeLa cells were seeded in 12-well plates and transfected with the nsp1 gene for 24 h, and stimulated with poly(I:C) for 12 h. Total RNA was extracted and mRNA expression was evaluated by qRT-PCR for IFN-β (A), ISG15 (B), and ISG56 (C). Results were normalized using β-actin mRNA and expressed as relative changes in mRNA levels with respect to those in cells without stimulation. Data are presented from three independent experiments, each in triplicate. Statistical analysis was performed by Student's *t* test. $^{*}P < 0.05$, $^{**}P < 0.01$, and $^{***}P < 0.001$.

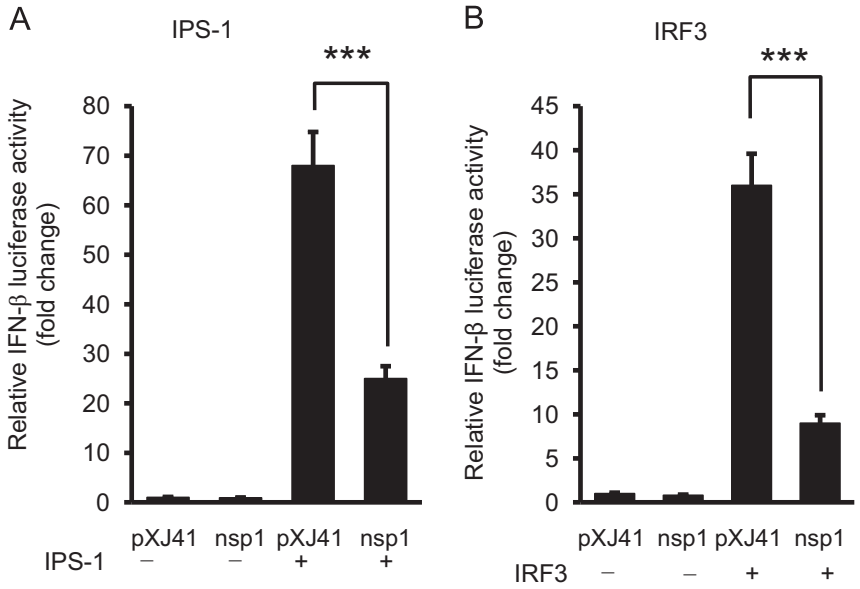

Fig. 6. *Disruption of IRF3-mediated IFN signaling by nsp1.* HeLa cells were seeded in 12-well plates and co-transfected with pMAVS/IPS-1 (A) or pIRF3 (B) along with the nsp1 gene, pRL-TK, and IFN-β-Luc reporter for 24 h. Cells were harvested to measure the firefly and renilla luciferase activities. Relative luciferase activity was defined as a ratio of the firefly luciferase to renilla luciferase activities. Data are presented as mean value ± standard deviation from three independent experiments. Statistical analysis was performed by Student's *t* test. $^{*}P < 0.05$, $^{**}P < 0.01$, and $^{***}P < 0.001$.

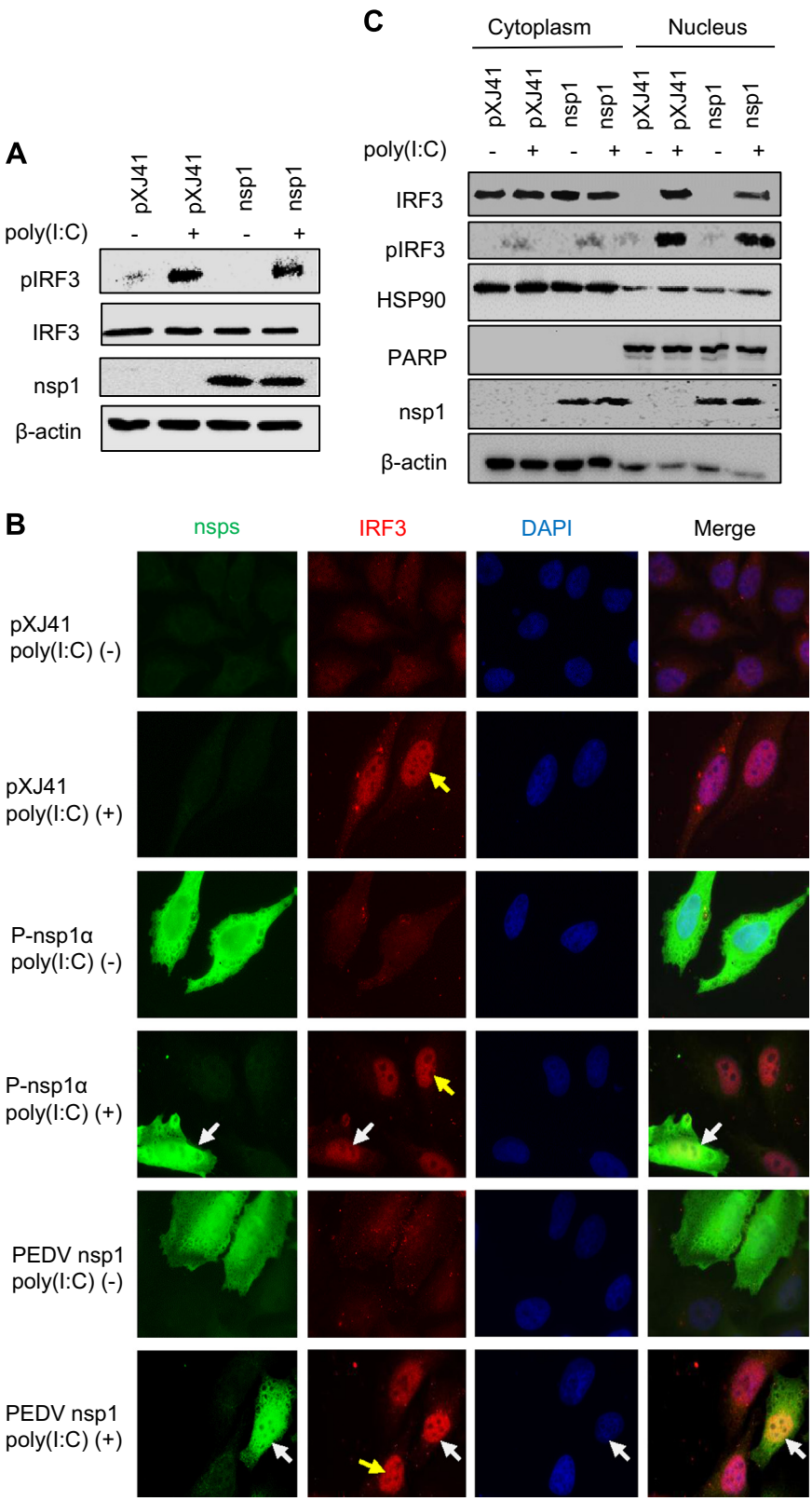

Fig. 7. *IRF3 phosphorylation and nuclear translocation by nsp1.* (A) HeLa cells were transfected with the nsp1-expressing plasmid for 24 h, followed by poly(I:C) stimulation for 8 h. Cells were lysed and subjected to Western blot to determine phosphorylated (p) IRF3. (B) Immunofluorescence staining for IRF3 nuclear translocation by nsp1. HeLa cells were transfected with the nsp1-expressing plasmid (2 μg/well) in 6-well plates for 24 h and stimulated by poly(I:C) for 8 h. Cells were fixed and incubated with rabbit anti-IRF3 pAb and rat anti-FLAG mAb for 1 h. PRRSV nsp1α does not inhibit the IRF3 nuclear localization and was used as a control. Alexa Fluor 594-conjugated goat anti-rabbit and 488-conjugated goat anti-mouse secondary antibodies were used to visualize IRF3 (red) and viral nsp1 (green), respectively. Nuclei (blue) were stained with DAPI. Yellow arrows indicate IRF3 localization in the nucleus in the absence of nsp1 expression. White arrows indicate IRF3 localization in the nucleus in nsp1-expressing cells. (C) Phosphorylation and nuclear localization of IRF3 by nsp1. HeLa cells were transfected with the PEDV nsp1 gene for 24 h, then stimulated with poly(I:C) for 8 h. Cells were lysed for nuclear–cytoplasmic fractionations and subcellular distribution of IRF3 and pIRF3. Hsp90 was used as a cytosolic protein marker and PARP was used as a nuclear protein marker.

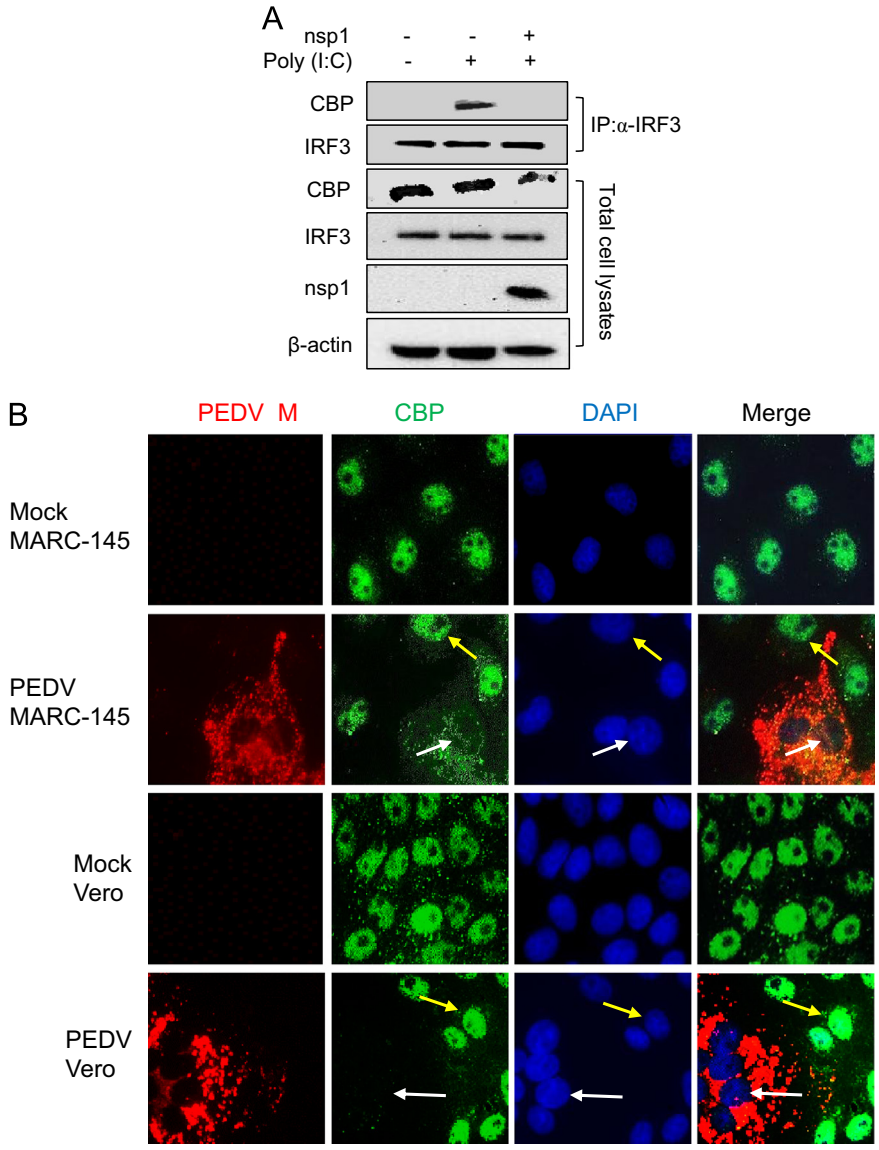

Fig. 8. *Degradation of CBP in PEDV-infected cells.* (A) Interruption of the IRF3 and CBP association by nsp1. HeLa cells were transfected with 2 μg/well of pXJ41-FLAG-nsp1 for 24 h and stimulated with poly(I:C) for 6 h. Cells were lysed and co-IP was carried out using rabbit anti-IRF3 and protein G-Agarose fast-flow beads (Millipore), followed by Western blot analysis using CBP antibody (panel 1, numbered from top) and IRF3 antibody (panel 2). Total cell lysates were probed for expression of CBP (panel 3), IRF3 (panel 4), nsp1 (panel 5), and β-actin as a loading control (panel 6). (B) Degradation of CBP in PEDV-infected cells. MARC-145 and Vero cells were seeded on coverslips placed on 6-well plates and grew to 80% confluency. Cells were infected with PEDV at an MOI of 0.1 for 24 h. Cells were then fixed and co-stained with rabbit anti-M pAb and mouse anti-CBP mAb. Alexa Fluor 594-conjugated goat anti-rabbit (red) and 488-conjugated goat anti-mouse (green) secondary antibodies were used to visualize protein expression. Nuclei (blue) were stained with DAPI. Yellow arrows indicate CBP in PEDV-uninfected cells. White arrows indicate CBP in PEDV-infected cells.

regions of the IFN-β promoter to assemble the basal transcription machinery complex together with NF-κB and other transcription factors to turn on the transcription of type I IFN genes (Honda and Taniguchi, 2006). Thus, the IRF3–CBP/p300 interaction for the assembly of enhanceosome is crucial for IFN expression. Since PEDV nsp1 did not block the IRF3 phosphorylation and nuclear translocation in our study, it was hypothesized that nsp1 might disrupt the formation of enhanceosome in the nucleus. To address this, the IRF3/CBP association was first examined in nsp1-expressing cells. Cells were transfected with the nsp1 gene and stimulated with poly(I:C) followed by co-immunoprecipitation using anti-IRF3 antibody and immunoblot with anti-CBP antibody. In unstimulated cells, CBP was undetectable due to the absence of IRF3/CBP association (Fig. 8A, left lane), but IRF3/CBP association became evident upon stimulation (Fig. 8A, middle lane). In nsp1-expressing cells however, the association of IRF3 and CBP disappeared even upon stimulation (Fig. 8A, right lane) and the detectable level of IRF3 remained unchanged (Fig. 8A, second panel). Absence of the association of CBP/IRF3 may occur when nsp1 binds to either IRF3 or CBP, or when IRF3 is unstable in the presence of nsp1. Since PEDV nsp1 was found to be a nuclear protein (Figs. 4A, B and 7B, C), nsp1 in the nucleus might interact with either IRF3 or CBP. However, neither the interaction between IRF3 and nsp1, nor between CBP and nsp1 was observed by co-immunoprecipitation in our study. IRF3 was also stable in the presence of nsp1 (Fig. 7A and C), indicating that the absence of IRF3/CBP association was not due to the instability of IRF3. Interestingly, the level of CBP was found to decrease in nsp1-expressing cells (Fig. 8A), leading us to investigate the degradation of CBP by nsp1.

Degradation of CBP by nsp1 is proteasome-dependent

Some viruses including HTLV, adenovirus, and an orthormyxovirus Thogoto interact with CBP to modulate type I IFN induction, suppress protein expression, or promote virus infection

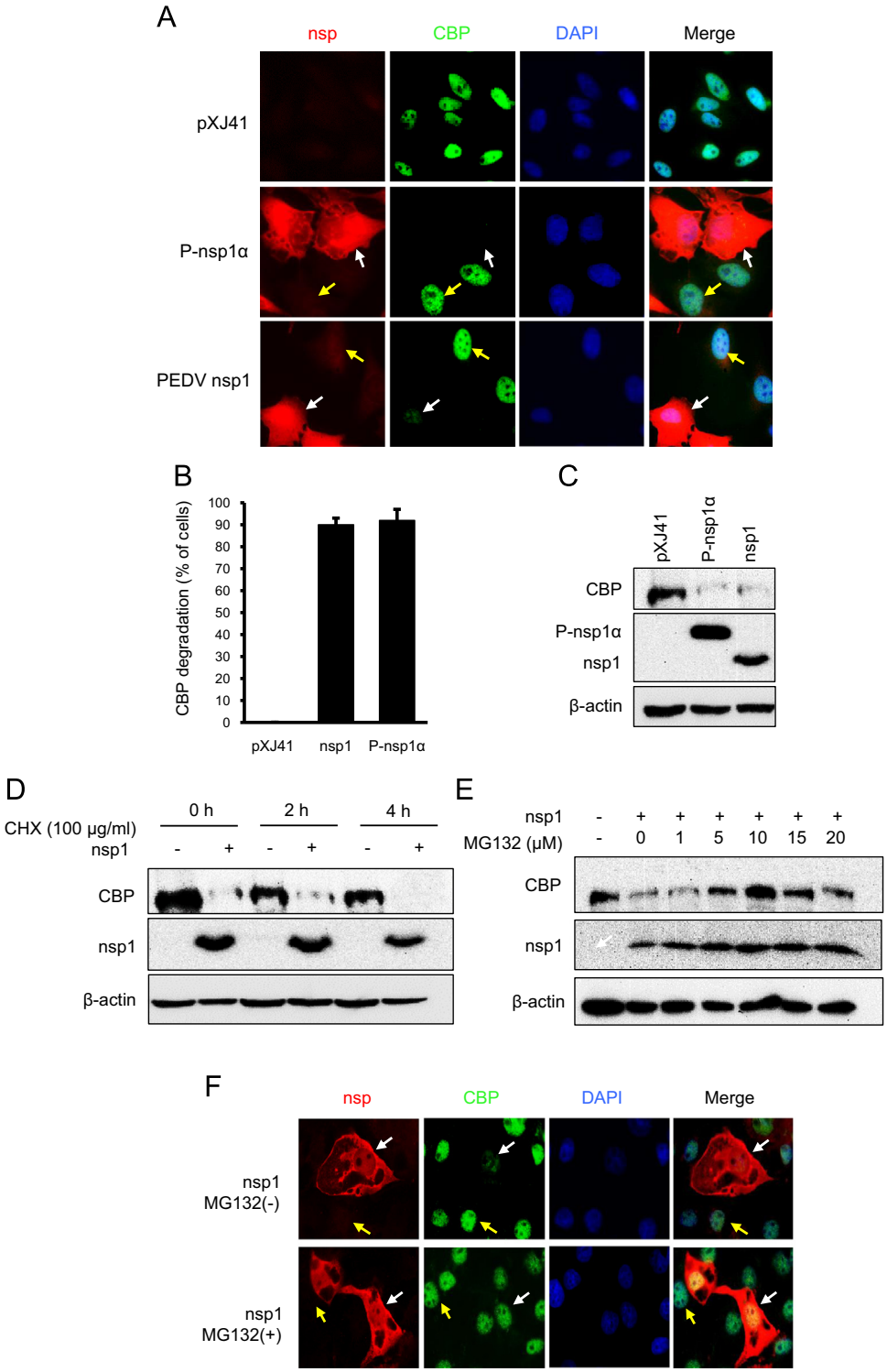

Fig. 9. *CBP degradation in the nucleus is mediated by nsp1.* (A) CBP degradation by nsp1 as determined by immunofluorescence assay. HeLa cells were transfected with PRRSV nsp1α which is known to degrade CBP in the nucleus, or PEDV nsp1. At 24 h post-transfection, cells were fixed and co-stained with rabbit anti-FLAG pAb and mouse anti-CBP mAb. Alexa Fluor 594-conjugated goat anti-rabbit and 488-conjugated goat anti-mouse (green) secondary antibodies were used to visualize nsp1 (red) and CBP (green). Nuclei (blue) were stained with DAPI. Yellow arrows indicate CBP in the absence of nsp1 expression, and white arrows indicates CBP in cells expressing viral nsp1. (B) Percent number of cells in which CBP was degraded by PEDV nsp1 and PRRSV nsp1α (P-nsp1α). Data are presented by % calculation of transfected cells showing more than 80% reduction of CBP fluorescent intensity compared to the control CBP staining out of 150 randomly chosen nsp1-expressing cells. (C) CBP degradation by nsp1 determined by Western blot. At 24 h transfection, cells lysates were prepared for Western blot using mouse anti-CBP mAb to examine the level of endogenous CBP. (D) PEDV nsp1-mediated degradation of CBP after cycloheximide (CHX) treatment. After 24 h transfection with the nsp1 gene, cells were treated with 100 μg/ml of CHX for indicated times, followed by Western blot using mouse anti-CBP mAb (top panel) and mouse anti-FLAG mAb for nsp1 detection (middle panel). (E) Inhibition of nsp1-mediated CBP degradation by MG132. After 24 h transfection with the nsp1 gene, HeLa cells were treated with MG132 at indicated concentrations for 16 h. Cells lysates were prepared and western blot was conducted using mouse anti-CBP mAb (top panel) or mouse anti-FLAG mAb (middle panel). (F) The CBP degradation by PEDV nsp1 in porcine intestinal epithelial cells IPEC-J2. IPEC-J2 cells were maintained as described in the Material and Methods, and transfected with the PEDV nsp1 gene. At 24 h post-transfection, cells were treated with or without 10 μM MG132 for 16 h, and then fixed for IFA. Yellow arrows indicate CBP in the absence of nsp1 expression, and white arrows indicates CBP in cells expressing viral nsp1.

(Ferrari et al., 2014; Jain et al., 2015; Jennings et al., 2005; Wurm et al., 2012; Zhang et al., 2008). Degradation of CBP has been described for the porcine arterivirus PRRSV as a strategy for IFN antagonism (Han and Yoo, 2014). Since the level of CBP was found to decrease in PEDV nsp1-expressing cells (Fig. 8A), CBP expression was validated in PEDV-infected cells by co-staining using anti-CBP antibody and anti-PEDV M pAb. In uninfected cells, CBP was predominately localized in the nucleus in MARC-145 and Vero cells (Fig. 8B, yellow arrows). In contrast, CBP was depleted in virus-infected cells (Fig. 8B, white arrows), demonstrating that the CBP was degraded by PEDV. We further sought to study whether the CBP degradation by PEDV was mediated by nsp1 protein. CBP was exclusively nuclear in control cells, whereas it was depleted in nsp1-expressing cells (Fig. 9A). PRRSV nsp1α is known to degrade CBP in the nucleus (Han and Yoo, 2014), and in PRRSV nsp1α-expressing cells, CBP was significantly depleted (Fig. 9A). The CBP degradation was quantified by examining the ratio of nsp1-expressing cells showing CBP degradation out of the chosen number of nsp1-expressing cells (Fig. 9B). Approximately 92% of PRRSV nsp1α-expressing cells showed more than 80% reduction of CBP, which is in consistent with the previous report (Han et al., 2013). For PEDV nsp1-expressing cells, approximately 90% cells showed more than 80% reduction of CBP, while no CBP reduction was observed in control cells. This finding was confirmed by western blot. In PEDV nsp1-expressing cells, CBP degradation was evident compared to that of control cells (Fig. 9C, top panel, lane 3). To eliminate a possibility that the reduction of CBP might be due to the short half-life of CBP, cyclohexamide (CHX) treatment was conducted (Fig. 9D). At 24 h post-transfection, cells were treated with CHX to shut down the new protein synthesis for indicated times followed by western blot. In nsp1-expressing cells, CBP reduction was evident at the beginning of CHX treatment, and further decreased by 2 h post-treatment. The CBP degradation was complete by 4 h post-treatment, whereas nsp1 and β-actin remained stable (Fig. 9D). Together, our data show that PEDV nsp1 was the viral protein contributing to the CBP degradation. Unlike PRRSV nsp1α, PEDV nsp1 does not contain a proteinase activity, and no direct interaction between CBP and nsp1 was identified in our study. It is thus unlikely that CBP would be a direct substrate of PEDV nsp1. Therefore, it was of interest to examine whether the CBP degradation was a proteasome-dependent process. The treatment with MG132 blocked the CBP degradation by nsp1. As little as 5 μM of MG132 was sufficient to inhibit the CBP degradation, and 10 μM was able to restore the CBP level back to the control level (Fig. 9E). To eliminate the CBP degradation by nsp1 was cell-type specific, we further tested the CBP degradation by nsp1 in pig intestinal epithelial cell line (IPEC-J2 cells), which reported to be susceptible to PEDV (Zhao et al., 2014). CBP degradation in nsp1-expressing cells was evident comparing to control cells (Fig. 9F, top panel). Additionally, The CBP degradation by nsp1 was also blocked by MG132 treatment in IPEC-J2 cells (Fig. 9F, bottom panel). This study indicates that the CBP degradation by PEDV nsp1 was proteasome-dependent in the nucleus.

Discussion

The innate immune system is the first line of host defense in response to viral infection. It initiates the production of type I IFNs and proinflammatory cytokines through the recognition of PAMPs by PRRs and establishes antiviral states which are highly effective on resisting and controlling infections. In turn, many viruses have developed strategies to counteract the host innate immune response to establish productive infection. Previous studies have shown that PEDV infection fail to induce the IFN-β promoter activation and that PLP2 (papain-like proteinase 2) of PEDV antagonizes the IFN response by deubiquitinating RIG-I and STING (Xing et al., 2013b). The PEDV N protein suppresses the IRF3 and NF-κB activities and antagonizes the IFN-β production by disrupting the interaction between IRF3 and TBK1 (Ding et al., 2014). On the contrary, a recent study shows that PEDV infection induces NF-κB activation in intestinal epithelial cells with the N protein as the activator (Cao et al., 2015b). In the present study, we have identified MARC-145 as PEDV permissive cells, and used these cells as a model to study the innate immune modulation for PEDV. We have shown the suppression of type I IFN production by PEDV, which is consistent with the recent finding in IECs (Cao et al., 2015a). We also have identified multiple viral proteins responsible for this suppression. We have further determined PEDV nsp1 as the viral component promoting CBP degradation in the nucleus via the proteasome-dependent pathway.

Many viruses in the order *Nidovirales* are able to modulate the host innate response, which plays an important role for their pathogenesis. In the family *Arteriviridae*, equine arteritis virus suppresses type I IFN production in equine endothelial cells (Go et al., 2014), and PRRSV also suppresses IFN production (Albina et al., 1998). PRRSV is susceptible to type I IFNs in cells and the suppression of type I IFN varies for different isolates (Albina et al., 1998; Lee et al., 2004; Overend et al., 2007). Mouse hepatitis virus (MHV), which is a *betacoronavirus,* induces a high level of IFN-α secretion by plasmacytoid dendritic cells (pDCs) during infection (Cervantes-Barragan et al., 2007). However, other cell types infected by MHV such as macrophages, microglia, and oligodendrocytes produce extremely low-levels of type I IFNs (Li et al., 2010; Roth-Cross et al., 2008; Zhou and Perlman, 2007). The MHV ns2 protein is dispensable for virus replication in cells but is required for induction of hepatitis in mouse (Schwarz et al., 1990). The 2′,5′-phosphodiesterase (PDE) activity of ns2 mediates the cleavage of 2′,5′-oligoadenylate and prevents the activation of RNase L, while enhancing viral growth and pathogenesis, thus ns2 is a viral IFN antagonist (Zhao et al., 2012). SARS-CoV, which is another member virus in the genus *betacoronavirus,* impairs the IFN response in virus-infected cells, and an IFN therapy has been suggested to be efficacious for SARS patients (Cinatl et al., 2004; Spiegel et al., 2005). MERS-CoV is also a *betacoronavirus,* and both MERS-CoV and SARS-CoV do not induce a pronounced IFN-response in polarized airway epithelial cells (Calu-3), alveolar adenocarcinoma cells (A549) and human monocyte-derived macrophages (Lau et al., 2013; Zhou et al., 2014; Zielecki et al., 2013). Even though the acute infection of TGEV induces a high-level of IFN-α in newborn pigs (La Bonnardiere and Laude, 1981), protein 7 counteracts the host antiviral response and influences viral pathogenesis (Cruz et al., 2011, 2013). The 7a protein of an *alphacoronavirus* feline infectious peritonitis virus is a type I IFN antagonist (Dedeurwaerder et al., 2014). Type I IFNs of chickens inhibits viral replication and respiratory illness of the *gammacoronavirus* infectious bronchitis coronavirus (IBV) (Pei et al., 2001). IBV delays the IFN response and the 3a and 3b accessory proteins have been identified as the IFN antagonists (Kint et al., 2015). Thus, modulation of type I IFN response seems to be a common evasion strategy of viruses in the order *Nidovirales*.

We have shown in the present study the direct evidence that PEDV indeed downregulates type I IFNs production during infection. PEDV suppresses the IFN-β and IRF3 activities. Since IRF3 is a key element in the production of type I IFNs, our finding leads to a hypothesis that PEDV modulation of type I IFNs production targets the IRF3 signaling pathway. Interestingly, PEDV normally activates the NF-κB activity in Vero E6 cells (Xing et al., 2013b). A recent study confirms that PEDV infection in intestinal epithelial cells induces NF-κB activation (Cao et al., 2015b). In that study, nuclear localization of p65 increases by PEDV after 12 h through 48 h.

However, activation of NF-κB during viral infection is generally an early event. For PRRSV, NF-κB is activated 30 min after infection (Fu et al., 2012). Thus, how PEDV modulates NF-κB activation during early time of infection needs to be further investigated. We have identified at least ten viral IFN antagonists and all ten proteins inhibit the IRF3 activity. Whether these IFN antagonists modulate the NF-κB activity needs to be further investigated. The PEDV N protein suppresses Sendai virus-induced NF-κB activity in a dose-dependent manner (Ding et al., 2014). In other study, N protein activates NF-κB in intestinal epithelial cells (Cao et al., 2015b). A possible explanation is that the NF-κB activation may be time-dependent and cell type-dependent. Together, the IRF3 signaling is likely the target by PEDV for type I IFNs modulation.

At least eleven viral proteins have been identified as IFN antagonists for SARS-CoV (Kindler and Thiel, 2014; Shi et al., 2014; Totura and Baric, 2012), whereas ten proteins have been identified for PEDV in our study. Thus, coronaviruses seem to arm with multiple antagonists. A possible explanation for such a functional redundancy is that coronavirus genomes are the largest RNA known to biology and undergo continuous genetic evolution. When a functional mutation occurs in a major antagonist, other antagonists may complement the function to ensure efficient replication and adaptation in hosts. For SARS-CoV, nsp1 is a multifunctional protein with the suppressive activity for IFN and blocks the phosphorylation of STAT1 and degrades host cell mRNA (Totura and Baric, 2012). SARS-CoV nsp14 and nsp15 works as exoribonuclease and endoribonuclease, respectively, thus specific digestion of dsRNAs and the consequent removal of RNA–PAMPs may lead to an inadequate activation of IFN response (Kindler and Thiel, 2014). SARS-CoV nsp16 contains 2′-O-methlytransferase activity and modifies the cap of viral RNAs in order to evade the detection by the host immune system (Totura and Baric, 2012). The SARS-CoV M protein impedes the formation of TRAF3 · TANK · TBK1/IKKϵ complex for suppression of type I IFN production (Siu et al., 2009, 2014). The PLP2 domain of SARS-CoV nsp3 negatively modulates type I IFN pathway and functions as a viral deubiquitinase. In our study, the full length PEDV nsp3 indeed inhibit the IFN activity. All ten antagonists identified for PEDV correspond to the respected antagonists of SARS-CoV. The corresponding proteins of PEDV may share the similar motifs and functions with those of SARS-CoV. Additionally, SARS-CoV encodes several accessory proteins. They are nonessential for viral replication but function as innate immune antagonists. For PEDV, ORF3 is the sole accessory protein, and a previous report shows that ORF3 functions as an ion channel protein and is relevant to infectivity and pathogenicity (Wang et al., 2012). ORF3 is nonessential for viral replication *in vitro* as shown by targeted RNA recombination (Li et al., 2013). In our study, ORF3 is a potent IFN antagonist. The viral antagonists may target different pathways of the host innate immune signaling and their synergistic effects may shut down the host innate immune response more efficiently during the course of infection.

CBP is a histone acetyltransferase and plays a key role in transcription regulation. The CBP/p300 coactivators interact with hundreds of transcription factors including STATs, c-Myc, PIAS1, p53, NF-κB, and IRF family (Bedford and Brindle, 2012; Goodman and Smolik, 2000; Long et al., 2004). For IFN expression, the assembly of an enhanceosome consisting of NF-κB, IRFs, ATF2/c-Jun, and the architectural protein HMG I(Y) is required in response to virus infection. The IFN enhanceosome recruits CBP/p300 for synergistic activation of transcription (Merika et al., 1998). Some viruses modulate the CBP activity for viral evasion. Two distinct regions in the simian virus 40 T antigen can independently alter the levels and loading of CBP/p300 transcripts onto polysomes for cell immortalization and transformation (Robles et al., 2013). African swine fever virus nuclear protein A238L inhibits the expression of TNF-α by displacing the CBP/p300 coactivators (Granja et al., 2006), and herpes simplex virus 1 (HSV-1) ICP0 protein recruits activated IRF3 and CBP/p300 to the nuclear foci, which may result in reduced transcription of IFN-β and inhibition of the host response (Melroe et al., 2007). HSV-1 VP16 protein inhibits NF-κB activation and interferes the recruitment of IRF3 to CBP to block the IFN-β production (Xing et al., 2013a). The ML protein of Thogoto virus interferes with IRF3 function without blocking its nuclear translocation but interrupts the association of IRF3 with CBP (Jennings et al., 2005), which is similar to the function of PEDV nsp1. The ML protein was later found to interact with the RNA polymerase II transcription factor IIB (TFIIB), however, this interaction hardly interferes the host general gene expression but strongly suppresses both the IRF3- and NF-κB-regulated promoter activities (Vogt et al., 2008). Thus, it is hypothesized that the virus-mediated CBP degradation may play a specific and key role for IFN modulation with a little impact on general cellular gene transcriptions. The degradation of CBP is a novel strategy for IFN modulation and has been extensively studied in the family of *Arteriviridae*, especially for PRRSV (Han and Yoo, 2014). For PRRSV nsp1α, CBP degradation is associated with the zinc-finger motif and is likely the key mechanism for IFN suppression (Han et al., 2013). For PEDV, nsp1 is the most potent IFN suppressor among all viral antagonists without affecting the IRF3 phosphorylation and nuclear localization. In line with this, PEDV infection depletes the endogenous CBP. Furthermore, PEDV nsp1 disrupts the association of CBP–IRF3 and degrades CBP in a proteasome-dependent manner. SARS-CoV nsp1 inhibits type I IFN production, induces host mRNA degradation, and suppresses host protein translation (Narayanan et al., 2008). However, the domains of SARS-CoV nsp1 responsible for suppression of host gene expression and type I IFN production are absent in PEDV nsp1 (Huang et al., 2011b; Narayanan et al., 2008). Even though nsp1s of *alphacoronavirus* and *betacoronavirus* share similar functions, they lack an overall sequence similarity and neither conserved motifs nor domains exist in viruses of *alphacoronaviruses*. Thus, it is plausible that nsp1 of *alphacoronaviruses* may have a distinct function regulating host innate immune responses and gene expression. TGEV nsp1 suppresses protein translation in cells and cell-free extracts. However, the suppression of protein translation by PEDV nsp1 may not be a general event since the β-actin shows the similar level of expression after infection and transfection. The lack of association of CBP-nsp1 and IRF3-nsp1 suggests that the CBP degradation by nsp1 is an indirect event that needs to be further determined. Similar to TGEV nsp1, the subcellular localization of PEDV nsp1 is nuclear–cytoplasmic. The sequence of PEDV nsp1 does not harbor any known nuclear localization signal, and thus nsp1 may piggy-bag a nuclear protein to enter the nucleus. The proteasome-dependent CBP degradation seems a unique viral tactic utilized to inhibit IFN-β production. It is of interest to study whether this is a common evasion strategy for coronaviruses.

CBP localizes in the PML nuclear bodies, which are discrete nuclear foci that are disrupted in acute promyelocytic leukemia (Boisvert et al., 2001; Doucas et al., 1999; LaMorte et al., 1998). The PML nuclear bodies dynamically colocalize with numerous proteins including CBP, PML, p53, Rb, sp100, DAXX, eIF4E, and SUMO (Jensen et al., 2001). Upon inhibition of proteasome activity, PML, sp100, EBNA-5, SUMO-1, and the 20S proteasome subunit move to the nucleolus, suggesting that proteasomal degradation occurs at the nuclear loci (Boddy et al., 1996). HAUSP, the ubiquitin-specific hydrolase in the PML nuclear bodies, removes ubiquitin moieties from proteins prior to proteasomal degradation (Everett et al., 1998). Thus, PML nuclear bodies may represent the sites where ubiquitinated proteins are processed by enzymes such as HAUSP prior to degradation in the nucleolus (St-Germain et al., 2008). Valproic acid, a histone deacetylase inhibitor, could induce CBP degradation through the ubiquitin–proteasome pathway, while increasing the colocalization of CBP with ubiquitin nuclear

speckles and with PML nuclear bodies (St-Germain et al., 2008), suggesting that PML nuclear bodies may be the sites for the ubiquitin-dependent degradation of CBP. It is of interest to examine whether PEDV nsp1 promotes ubiquitination of CBP for degradation in the nucleus and whether this degradation associates with PML nuclear bodies.

PEDV infects Vero cells and MARC-145 cells. Porcine amino peptidase N (pAPN) has been identified as the major cell entry receptor for PEDV (Li et al., 2007; Nam and Lee, 2010). Transient expression of pAPN confers PEDV non-permissive canine kidney cells (MDCK) to be permissive for PEDV infection. pAPN also increases the PEDV infectivity in porcine small intestine epithelial cells (IECs) (Cong et al., 2015). The respiratory tract may support PEDV infection in pigs and the virus infects and replicates in transformed alveolar macrophages (3D4) *in vitro* (Park and Shin, 2014). Primate APN or receptor-independent pathways in Vero and MARC-145 cells may complement the function of pAPN for PEDV infection (Taguchi and Matsuyama, 2002).

In summary, we have shown the suppression of type I IFN production by PEDV and have identified specific viral IFN antagonists. Among these antagonists, nsp1 is the most potent protein and functions to degrade CBP in the nucleus. Our data provides a novel insight into the understanding of the immune evasion strategy of PEDV.

Material and methods

Cells, viruses, antibodies and chemicals

HeLa cells (NIH AIDS Research and Reference Reagent Program, Germantown, MD) and MARC-145 cells (Kim et al., 1993) were maintained in minimum essential medium (MEM) and Dulbecco's modified Eagle's medium (DMEM) (Mediatech, Manassas, VA), respectively, supplemented with 10% heat inactivated fetal bovine serum (FBS) (Hyclone, Logan, UT). Vero cells (ATCC® CCL-81™) were grown in DMEM supplemented with 10% FBS. The IPEC-J2 cell line is a continuous line of epithelial cells derived from the jejunum of a 12 h old, unsuckled mixed breed piglet and was obtained from Dr. Anthony Blikslager (North Carolina State University). IPEC-J2 was maintained in DMEM/F12 with 5% FBS supplemented with 5 μg/ml of insulin/selenium/transferrin (Life Technologies), and 5 ng/ml of epidermal growth factor (Life Technologies). PEDV (USA/Colorado/2013; GenBank: KF272920) was obtained from Agricultural Research Service US Department of Agriculture (Ames, IA). PEDV was propagated in MARC-145 cells with DMEM or Vero cells with MEM supplemented with 0.3% tryptose phosphate broth (Sigma, St. Louis, MO), 0.02% yeast extract (Teknova, Hollister, CA), and trypsin 250 (Sigma-Aldrich, St. Louis, MO). The trypsin concentration was 2 μg/ml for MARC-145 cells and 5 μg/ml in Vero cells. The recombinant vesicular stomatitis virus expressing green fluorescent protein (VSV–GFP) was kindly provided by Dr. A. Garcia-Sastre (Mount Sinai Hospital, New York, NY).

Polyinosinic:polycytidylic acid [poly(I:C)], DAPI (4′, 6-diamidino-2-phenylindole), and cycloheximide (CHX), rat anti-FLAG mAb were purchased from Sigma (St. Louis, MO). Human recombinant IFN-β and MG132 were purchased from Calbiochem (San Diego, CA). Anti-β-actin mAb (sc-47778), anti-CBP mAb (sc-7300), anti-hsp90 mAb (sc-69703), anti-PARP pAb (sc-7150), and anti-IRF3 pAb (sc-9082) were purchased from Santa Cruz Biotechnologies Inc. (Santa Cruz, CA). Anti-phospho-IRF3 PAb (Ser396) were purchased from Cell Signaling (Danvers, MA). Rabbit anti-PEDV M pAb was kindly provided by Dr. Y. Fang (Kansas State University, Manhattan, KS). Mouse anti-PEDV N mAb was purchased from Medgene (Brookings, SD). Lipofectamine 2000 Transfection Reagent was purchased from Invitrogen (Carlsbad, CA). QIAamp Viral RNA mini kit and RNeasy mini kit were purchased from QIAGEN (Venlo, Limburg). Power SYBR Green PCR master mix was purchased from Life Technologies (Carlsbad, CA). Alexa Fluor 594-conjugated (goat anti-rabbit, red) and 488-conjugated (goat anti-mouse, green) secondary antibodies and Pierce™ ECL Western blotting substrate were purchased from Thermo Scientific (Waltham, MA).

Plasmids and gene cloning

The firefly luciferase genes were used as reporters with its expression under the control of various promoters as indicated below. The plasmid pIFN-β-Luc contains the entire IFN-β enhancer-promoter. The plasmid p4 × IRF3-Luc contains four copies of IRF3 binding region PRD I–III of the IFN-β promoter. pIFN-β-Luc and p4 × IRF3-Luc were obtained from Dr. Stephan Ludwig at Heinrich-Heine-Universität, Düsseldorf, Germany (Ehrhardt et al., 2004). The Renilla luciferase plasmid pRL-TK (Promega) contains the herpes simplex virus thymidine kinase (HSV-tk) promoter and was included in all experiments to serve as an internal control. Active stimulator pMAVS/IPS-1 was obtained from Dr. J. Shisler (University of Illinois, Urbana, IL). pIRF3 was kindly provided by Dr. B. Gotoh (University of Fukui, Fukui, Japan). pDsRed2-ER and pDsRed2-Mito were purchased from Clontech.

Plasmids with the FLAG tag for expression of nsp1 through nsp16, and the S, S1, S2, ORF3, E, M and N genes were cloned from the viral genomic RNA by standard reverse transcription and PCR techniques using indicated primers (Table 1). Twenty-three viral genes were amplified and cloned into the eukaryotic expression vector pXJ41 using indicated restriction enzymes. The nsp1 to nsp16, ORF3, and N genes were expressed as fusion proteins with the N-terminal FLAG tag, and the S, S1, S2, E, and M genes were expressed as fusion proteins with the C-terminal FLAG tag to avoid the functional disruption of the signal sequence. The constructs were confirmed by sequencing, immunofluorescence, and western blot. PRRSV nsp1α and its cystine mutant P-nsp1α(m) (C28S) are described elsewhere (Han et al., 2013; Song et al., 2010).

DNA transfection and luciferase reporter assay

HeLa cells were seeded in 12-well plates and grown to 80% confluency prior to transfection. Individual viral protein genes, luciferase reporters, and pRL-TK as an internal control were transfected at a ratio of 10:10:1 in a total of 1.05 μg/well using Lipofectamine 2000 according to the manufacturer's instruction (Invitrogen). At 24 h post-transfection, cells were stimulated by transfection with 0.5 μg/well of poly(I:C) for 12 h. Cells were then lysed and luciferase assays were performed using the Dual Luciferease assay system according to the manufacturer's instructions (Promega). Values were normalized using the Renilla luciferase activity as the internal control and presented in fold-changes. Three independent assays were performed with each assay in triplicate.

Relative quantitative real-time RT-PCR

Total RNA was extracted from HeLa or MARC-145 cells using RNeasy mini kit according to the manufacturer's instructions (QIAGEN). The RNA was treated with DNase I to remove contaminating genomic DNA. Reverse transcription (RT) reaction was performed with 1 μg of total RNA using random primers and M-MLV reverse transcriptase (Invitrogen). SYBR Green real-time PCR was conducted in the ABI 7500 real-time PCR system according to the manufacturer's instructions (Life Technologies). The real-time PCR primers for IFN-β, ISG15, ISG56 and β-actin were listed in

Table 1
Primers used for the cloning of PEDV nonstructural and structural genes (PEDV strain USA/Colorado/2013).

Primer	Sequence (5'-3')
nsp1-F	GCCGAATTCACCATG*GATTACAAGGATGACGACGATAAG*ATGGCTAGCAACCATG
nsp1-R	GCCCTCGAGCTAACCACCACGACG
nsp2-F	GCCGGATCCACCATG*GATTACAAGGATGACGACGATAAG*AACATCGTGCCAG
nsp2-R	GCCGGTACCCTAACCACCTTTCTTC
nsp3-F	AGTCTCGAGACCATG*GATTACAAGGATGACGACGATAAG*GGTGATGTCAAATTC
nsp3-R	GCCAGATCTCTATGCACCCTTCTTATTTG
nsp4-F	GCCGGATCCACCATG*GATTACAAGGATGACGACGATAAG*GGTCTTCCTAGTTTTTC
nsp4-R	GCCCTCGAGCTACTGTAGAGTTGAATTG
nsp5-F	GCCGAATTCACCATG*GATTACAAGGATGACGACGATAAG*GCTGGCTTGCGTAAG
nsp5-R	GCCCTCGAGCTACTGAAGATTAACGCC
nsp6-F	GCCGAATTCACCATG*GATTACAAGGATGACGACGATAAG*AGTGGTTATGTTTC
nsp6-R	GCCCTCGAGCTACTGAACGGAAG
nsp7-F	GCCGAATTCACCATG*GATTACAAGGATGACGACGATAAG*TCTAAACTGACTG
nsp7-R	GCCCTCGAGCTACTGCAACATAC
nsp8-F	GCCGAATTCACCATG*GATTACAAGGATGACGACGATAAG*AGTGTTGCATCTAC
nsp8-R	GCCCTCGAGCTACTGGAGCTTGAC
nsp9-F	GCCGAATTCACCATG*GATTACAAGGATGACGACGATAAG*AATAATGAAATTATTCC
nsp9-R	GCCCTCGAGCTACTGCAAGCGTAC
nsp10-F	GCCGAATTCACCATG*GATTACAAGGATGACGACGATAAG*GCTGGTAAACAAACAG
nsp10-R	GCCCTCGAGCTATTGCATAATGGATC
nsp12-F	GCCGGATCCACCATG*GATTACAAGGATGACGACGATAAG*AGCACTGATATGGC
nsp12-R	GCCCTCGAGCTATTGTAAAACTGCAG
nsp13-F	GCCGAATTCACCATG*GATTACAAGGATGACGACGATAAG*TCTGCAGGGCTTTGTG
nsp13-R	GCCCTCGAGCTACTGCAAATCAG
nsp14-F	GCCGAATTCACCATG*GATTACAAGGATGACGACGATAAG*GCTAATGAGGGTTGTG
nsp14-R	GCCCTCGAGCTATTGCAAATTGTTAC
nsp15F	GCCGAATTCACCATG*GATTACAAGGATGACGACGATAAG*GGTCTTGAGAACATTGC
nsp15R	GCCCTCGAGCTACTGAAGTTGCGGAT
nsp16F	GCCGAATTCACCATG*GATTACAAGGATGACGACGATAAG*GCCAGTGAATGGAAG
nsp16R	GCCCTCGAGTCATTTGTTTACGTTG
S-F	GCCGAATTCACCATGAAGTCTTTAACCTAC
S-R	GCCCTCGAGTCA*CTTATCGTCGTCATCCTTGTAATC*CTGCACGTGGACCTTTTC
S1-F	GCCGAATTCACCATGATGAAGTCTTTAACCTAC
S1-R	GCCCTCGAGTCA*CTTATCGTCGTCATCCTTGTAATC*AATACTCATACTAAAG
S2-F	GCCGAATTCACCATGAGGACAGAATATTTACAG
S2-R	GCCCTCGAGTCA*CTTATCGTCGTCATCCTTGTAATC*CTGCACGTGGACCTTTTC
ORF3-F	GCCGAATTCACCATG*GATTACAAGGATGACGACGATAAG*ATGTTTCTTGGAC
ORF3-R	GCCCTCGAGTCATTCACTAATTGTAG
E-F	GCCGAATTCACCATGCTACAATTAGTG
E-R	GCCCTCGAGTCA*CTTATCGTCGTCATCCTTGTAATC*TACGTCAATAACAGTAC
M-F	GCCGAATTCACCATGTCTAACGGTTCTATTC
M-R	GCCCTCGAGTCA*CTTATCGTCGTCATCCTTGTAATC*GACTAAATGAAGCAC
N-F	GCCGGATCCACCATG*GATTACAAGGATGACGACGATAAG*ATGGCTTCTGTCAG
N-R	GCCCTCGAGTCAATTTCCTGTGTCGAAG

Restriction enzyme recognition sequences are underlined. The FLAG tag is italicized and underlined.

Table 2
Primers used for relative quantitative real-time RT-PCR.

Primer	Sequence (5'-3')
IFN-β-F	GATTTATCTAGCACTGGCTGG
IFN-β-R	CTTCAGGTAATGCAGAATCC
ISG15-F	CACCGTGTTCATGAATCTGC
ISG15-R	CTTTATTTCCGGCCCTTGAT
ISG56-F	CCTCCTTGGGTTCGTCTACA
ISG56-R	GGCTGATATCTGGGTGCCTA
β-actin-F	ATCGTGCGTGACATTAAG
β-actin-R	ATTGCCAATGGTGATGAC

Table 2. For each sample, the β-actin gene was amplified and used as an internal control. Specific amplification was confirmed by sequencing PCR products. The threshold cycle for target genes and the difference between their C_t values (ΔC_t) were determined. The relative transcript levels of target gene are equal to $2^{-\Delta\Delta Ct}$ threshold method (Livak and Schmittgen, 2001) and are shown as fold changes relative to the respective untreated control samples.

VSV–GFP interferon bioassay

HeLa cells were seeded in 6-well plates and transfected with 2 μg of plasmid. At 24 h post-transfection, cells were stimulated by transfection with 1 μg of poly(I:C) for 12 h. Supernatants were harvested for bioassay. For PEDV, MARC-145 cells were infected with PEDV at an MOI of 1 for 12 h prior to poly(I:C) stimulation. Supernatants from virus-infected cells were UV-irradiated for 30 min to remove infectivity prior to bioassay. The supernatants were then serially diluted by 2-fold. MARC-145 cells were freshly grown in 96-well plates and incubated with 100 μl of each dilution for 24 h. Cells were then infected in 100 μl of VSV–GFP at 10^4 PFU/ml for 16 h and GFP expression was examined by inverted fluorescence microscopy (Nikon Eclipse TS100, 10 × 10). Each dilution was examined twice in triplicate each.

Indirect immunofluorescence assay (IFA) and confocal microscopy

Cells were seeded on coverslips and transfected with plasmids or infected with PEDV. For transfection of HeLa cells, total 2 μg of individual plasmids were transfected for 24 h using Lipofectamine

2000 according to the manufacturer's instructions (Invitrogen). Cells were then either treated with poly(I:C) for 12 h or IFN-β for 40 min. Cells were fixed with 4% paraformaldehyde in PBS overnight at 4 °C and permeabilized using 0.1% Triton X-100 for 15 min at room temperature (RT). After blocking with 1% BSA in PBS at RT for 30 min, cells were incubated with a primary antibody in PBS for 1–3 h. Cells were then washed three times with PBS and incubated with Alexa Fluor 488-labeled anti-mouse secondary antibody, or Alexa Fluor 594-labeled anti-rabbit secondary antibody (Thermo Scientific) for 1 h at RT in the dark. Cells were incubated with DAPI for 5 min at RT for nuclear staining. After washing with PBS, cover slips were mounted on microscope slides using Fluoromount-G mounting medium (Southern Biotech, Birmingham, AL), and visualized by fluorescence microscopy (Nikon Eclipse TS100). Confocal microscopy was conducted as described elsewhere (Kannan et al., 2009).

Cell fractionation

HeLa cells were seeded in 6-well plates to 80% confluency and transfected with 2 μg/well of nsp1 plasmid for 24 h. Cells were stimulated with 1 μg of poly(I:C) for 12 h and fractionated using the Nuclear/Cytosol Fractionation kit (BioVision, Milpitas, CA) with minor modifications. Briefly, cells were washed with cold PBS and collected using cell scrapers in 1 ml of cold PBS. Cell pellets were resuspended in 200 μl CEB-A buffer and incubated on ice for 10 min. After addition of CEB-B, tubes were vortexed and incubated on ice for 1 min. The cell lysates were then centrifuged at 4 °C 5 min at 16,000*g* and supernatants were collected as the cytosolic fraction. The cell pellets were suspended in NEB buffer and vortexed for 30 s and repeated 5 times every 10 min. The nuclear pellets were finally centrifuged for 10 min at 4 °C 16,000*g* and kept the supernatants as the nuclear fraction.

Western blot

Cells were harvested in RIPA buffer [20 mM Tris (pH 7.5), 150 mM NaCl, 1 mM EDTA, 1 mM phenylmethanesulphonyl fluoride (PMSF), 0.1% SDS, 0.5% sodium deoxycholate, 1% NP-40] containing the proteinase inhibitors cocktail (Promega). Cells were frozen–thawed, collected in the pre-cold tubes, and centrifuged to remove insoluble components. Total protein concentration was determined using Pierce BCA protein assay kit (Thermo Scientific). Equal amounts of proteins were resolved by SDS-PAGE and blotted to PVDF membranes (Millipore). After blocking with 5% nonfat dry milk in TBST (0.05% Tween-20) for 1 h, membranes were incubated with a primary antibody in TBST containing 5% nonfat dry milk overnight at 4 °C, followed by washing and incubation with horseradish peroxidase (HRP)-conjugated secondary antibody for 1 h at RT. The membrane was visualized using Pierce ECL Western Blotting Substrate (Thermo Scientific) and images were taken by FluorChem™ R System according to the manufacturer's instructions (ProteinSimple).

Co-immunoprecipitation

Co-immunoprecipitation (co-IP) was performed as described previously with modifications (Kim et al., 2010). Gene-transfected cells were lysed in lysis buffer [50 mM Tris (pH 8.0), 150 mM NaCl, 5 mM Na_3VO_4, 1 mM PMSF, 100 mg/ml leupetin, 1% NP-40, 10% glycerol] supplemented proteinase inhibitors cocktail (Promega). Cell lysates were clarified by centrifugation at 4 °C for 10 min at 16,000*g*. Supernatants were transferred to fresh tubes and incubated with either FLAG- or IRF3-antibody at 4 °C overnight, followed by incubation with protein G Agarose beads (Fast Flow, Millipore) at 4 °C for 4 h. Pellets were collected by centrifugation and washed for five times. The final pellets were eluted with Laemmli sample buffer (Bio-Rad) and were subjected to western blot.

Statistical analysis

Student's *t*-test was used for all statistical analyses. Asterisks indicate the statistical significance. $^{*}P<0.05$, $^{**}P<0.01$ and $^{***}P<0.001$.

Acknowledgments

This study was supported by Agriculture and Food Research Initiative (AFRI) Competitive Grant no. 2013-67015-21243 of the USDA-NIFA and the USDA HATCH and Multistate Research Fund.

References

Albina, E., Carrat, C., Charley, B., 1998. Interferon-alpha response to swine arterivirus (PoAV), the porcine reproductive and respiratory syndrome virus. J. Interferon Cytokine Res. 18, 485–490.
Bedford, D.C., Brindle, P.K., 2012. Is histone acetylation the most important physiological function for CBP and p300? Aging 4, 247–255.
Boddy, M.N., Howe, K., Etkin, L.D., Solomon, E., Freemont, P.S., 1996. PIC 1, a novel ubiquitin-like protein which interacts with the PML component of a multiprotein complex that is disrupted in acute promyelocytic leukaemia. Oncogene 13, 971–982.
Boisvert, F.M., Kruhlak, M.J., Box, A.K., Hendzel, M.J., Bazett-Jones, D.P., 2001. The transcription coactivator CBP is a dynamic component of the promyelocytic leukemia nuclear body. J. Cell Biol. 152, 1099–1106.
Cao, L., Ge, X., Gao, Y., Herrler, G., Ren, Y., Ren, X., Li, G., 2015a. Porcine epidemic diarrhea virus inhibits dsRNA-induced interferon-β production in porcine intestinal epithelial cells by blockade of the RIG-I-mediated pathway. Virol. J. 12, 127.
Cao, L., Ge, X., Gao, Y., Ren, Y., Ren, X., Li, G., 2015b. Porcine epidemic diarrhea virus infection induces NF-kappaB activation through the TLR2, TLR3, and TLR9 pathways in porcine intestinal epithelial cells. J. Gen. Virol. 96, 1757–1767.
Cervantes-Barragan, L., Zust, R., Weber, F., Spiegel, M., Lang, K.S., Akira, S., Thiel, V., Ludewig, B., 2007. Control of coronavirus infection through plasmacytoid dendritic-cell-derived type I interferon. Blood 109, 1131–1137.
Chen, J., Liu, X., Shi, D., Shi, H., Zhang, X., Li, C., Chi, Y., Feng, L., 2013. Detection and molecular diversity of spike gene of porcine epidemic diarrhea virus in China. Viruses 5, 2601–2613.
Chen, Q., Li, G., Stasko, J., Thomas, J.T., Stensland, W.R., Pillatzki, A.E., Gauger, P.C., Schwartz, K.J., Madson, D., Yoon, K.J., Stevenson, G.W., Burrough, E.R., Harmon, K.M., Main, R.G., Zhang, J., 2014. Isolation and characterization of porcine epidemic diarrhea viruses associated with the 2013 disease outbreak among swine in the United States. J. Clin. Microbiol. 52, 234–243.
Cinatl Jr., J., Michaelis, M., Scholz, M., Doerr, H.W., 2004. Role of interferons in the treatment of severe acute respiratory syndrome. Expert Opin. Biol. Ther. 4, 827–836.
Cong, Y., Li, X., Bai, Y., Lv, X., Herrler, G., Enjuanes, L., Zhou, X., Qu, B., Meng, F., Cong, C., Ren, X., Li, G., 2015. Porcine aminopeptidase N mediated polarized infection by porcine epidemic diarrhea virus in target cells. Virology 478, 1–8.
Cruz, J.L., Becares, M., Sola, I., Oliveros, J.C., Enjuanes, L., Zuniga, S., 2013. Alphacoronavirus protein 7 modulates host innate immune response. J. Virol. 87, 9754–9767.
Cruz, J.L., Sola, I., Becares, M., Alberca, B., Plana, J., Enjuanes, L., Zuniga, S., 2011. Coronavirus gene 7 counteracts host defenses and modulates virus virulence. PLoS Pathog. 7, e1002090.
Debouck, P., Pensaert, M., 1980. Experimental infection of pigs with a new porcine enteric coronavirus, CV 777. Am. J. Vet. Res. 41, 219–223.
Dedeurwaerder, A., Olyslaegers, D.A., Desmarets, L.M., Roukaerts, I.D., Theuns, S., Nauwynck, H.J., 2014. ORF7-encoded accessory protein 7a of feline infectious peritonitis virus as a counteragent against IFN-alpha-induced antiviral response. J. Gen. Virol. 95, 393–402.
Desmyter, J., Melnick, J.L., Rawls, W.E., 1968. Defectiveness of interferon production and of rubella virus interference in a line of African green monkey kidney cells (Vero). J. Virol. 2, 955–961.
Ding, Z., Fang, L., Jing, H., Zeng, S., Wang, D., Liu, L., Zhang, H., Luo, R., Chen, H., Xiao, S., 2014. Porcine epidemic diarrhea virus nucleocapsid protein antagonizes beta interferon production by sequestering the interaction between IRF3 and TBK1. J. Virol. 88, 8936–8945.
Doucas, V., Tini, M., Egan, D.A., Evans, R.M., 1999. Modulation of CREB binding protein function by the promyelocytic (PML) oncoprotein suggests a role for nuclear bodies in hormone signaling. Proc. Natl. Acad. Sci. U.S.A. 96, 2627–2632.
Dragan, A.I., Hargreaves, V.V., Makeyeva, E.N., Privalov, P.L., 2007. Mechanisms of activation of interferon regulator factor 3: the role of C-terminal domain

phosphorylation in IRF-3 dimerization and DNA binding. Nucleic Acids Res. 35, 3525–3534.
Duarte, M., Gelfi, J., Lambert, P., Rasschaert, D., Laude, H., 1993. Genome organization of porcine epidemic diarrhoea virus. Adv. Exp. Med. Biol. 342, 55–60.
Ehrhardt, C., Kardinal, C., Wurzer, W.J., Wolff, T., von Eichel-Streiber, C., Pleschka, S., Planz, O., Ludwig, S., 2004. Rac1 and PAK1 are upstream of IKK-epsilon and TBK-1 in the viral activation of interferon regulatory factor-3. FEBS Lett. 567, 230–238.
Everett, R.D., Freemont, P., Saitoh, H., Dasso, M., Orr, A., Kathoria, M., Parkinson, J., 1998. The disruption of ND10 during herpes simplex virus infection correlates with the Vmw110- and proteasome-dependent loss of several PML isoforms. J. Virol. 72, 6581–6591.
Ferrari, R., Gou, D., Jawdekar, G., Johnson, S.A., Nava, M., Su, T., Yousef, A.F., Zemke, N.R., Pellegrini, M., Kurdistani, S.K., Berk, A.J., 2014. Adenovirus small E1A employs the lysine acetylases p300/CBP and tumor suppressor Rb to repress select host genes and promote productive virus infection. Cell Host Microbe 16, 663–676.
Fitzgerald, K.A., McWhirter, S.M., Faia, K.L., Rowe, D.C., Latz, E., Golenbock, D.T., Coyle, A.J., Liao, S.M., Maniatis, T., 2003. IKKepsilon and TBK1 are essential components of the IRF3 signaling pathway. Nat. Immunol. 4, 491–496.
Fu, Y., Quan, R., Zhang, H., Hou, J., Tang, J., Feng, W.H., 2012. Porcine reproductive and respiratory syndrome virus induces interleukin-15 through the NF-kappaB signaling pathway. J. Virol. 86, 7625–7636.
Go, Y.Y., Li, Y., Chen, Z., Han, M., Yoo, D., Fang, Y., Balasuriya, U.B., 2014. Equine arteritis virus does not induce interferon production in equine endothelial cells: identification of nonstructural protein 1 as a main interferon antagonist. Biomed. Res. Int. 2014, 420658.
Goodman, R.H., Smolik, S., 2000. CBP/p300 in cell growth, transformation, and development. Genes Dev. 14, 1553–1577.
Granja, A.G., Nogal, M.L., Hurtado, C., Del Aguila, C., Carrascosa, A.L., Salas, M.L., Fresno, M., Revilla, Y., 2006. The viral protein A238L inhibits TNF-alpha expression through a CBP/p300 transcriptional coactivators pathway. J. Immunol. 176, 451–462.
Han, M., Du, Y., Song, C., Yoo, D., 2013. Degradation of CREB-binding protein and modulation of type I interferon induction by the zinc finger motif of the porcine reproductive and respiratory syndrome virus nsp1alpha subunit. Virus Res. 172, 54–65.
Han, M., Yoo, D., 2014. Modulation of innate immune signaling by nonstructural protein 1 (nsp1) in the family Arteriviridae. Virus Res. 194, 100–109.
Hofmann, M., Wyler, R., 1988. Propagation of the virus of porcine epidemic diarrhea in cell culture. J. Clin. Microbiol. 26, 2235–2239.
Honda, K., Taniguchi, T., 2006. IRFs: master regulators of signalling by Toll-like receptors and cytosolic pattern-recognition receptors. Nat. Rev. Immunol. 6, 644–658.
Huang, C., Lokugamage, K.G., Rozovics, J.M., Narayanan, K., Semler, B.L., Makino, S., 2011a. Alphacoronavirus transmissible gastroenteritis virus nsp1 protein suppresses protein translation in mammalian cells and in cell-free HeLa cell extracts but not in rabbit reticulocyte lysate. J. Virol. 85, 638–643.
Huang, C., Lokugamage, K.G., Rozovics, J.M., Narayanan, K., Semler, B.L., Makino, S., 2011b. SARS coronavirus nsp1 protein induces template-dependent endonucleolytic cleavage of mRNAs: viral mRNAs are resistant to nsp1-induced RNA cleavage. PLoS Pathog. 7, e1002433.
Huang, C., Zhang, Q., Guo, X.K., Yu, Z.B., Xu, A.T., Tang, J., Feng, W.H., 2014. Porcine reproductive and respiratory syndrome virus nonstructural protein 4 antagonizes beta interferon expression by targeting the NF-kappaB essential modulator. J. Virol. 88, 10934–10945.
Jain, P., Lavorgna, A., Sehgal, M., Gao, L., Ginwala, R., Sagar, D., Harhaj, E.W., Khan, Z. K., 2015. Myocyte enhancer factor (MEF)-2 plays essential roles in T-cell transformation associated with HTLV-1 infection by stabilizing complex between tax and CREB. Retrovirology 12, 23.
Jennings, S., Martinez-Sobrido, L., Garcia-Sastre, A., Weber, F., Kochs, G., 2005. Thogoto virus ML protein suppresses IRF3 function. Virology 331, 63–72.
Jensen, K., Shiels, C., Freemont, P.S., 2001. PML protein isoforms and the RBCC/TRIM motif. Oncogene 20, 7223–7233.
Junwei, G., Baoxian, L., Lijie, T., Yijing, L., 2006. Cloning and sequence analysis of the N gene of porcine epidemic diarrhea virus LJB/03. Virus Genes 33, 215–219.
Kannan, H., Fan, S., Patel, D., Bossis, I., Zhang, Y.J., 2009. The hepatitis E virus open reading frame 3 product interacts with microtubules and interferes with their dynamics. J. Virol. 83, 6375–6382.
Kawai, T., Akira, S., 2011. Toll-like receptors and their crosstalk with other innate receptors in infection and immunity. Immunity 34, 637–650.
Kim, H.S., Kwang, J., Yoon, I.J., Joo, H.S., Frey, M.L., 1993. Enhanced replication of porcine reproductive and respiratory syndrome (PRRS) virus in a homogeneous subpopulation of MA-104 cell line. Arch. Virol. 133, 477–483.
Kim, O., Sun, Y., Lai, F.W., Song, C., Yoo, D., 2010. Modulation of type I interferon induction by porcine reproductive and respiratory syndrome virus and degradation of CREB-binding protein by non-structural protein 1 in MARC-145 and HeLa cells. Virology 402, 315–326.
Kindler, E., Thiel, V., 2014. To sense or not to sense viral RNA – essentials of coronavirus innate immune evasion. Curr. Opin. Microbiol. 20, 69–75.
Kint, J., Fernandez-Gutierrez, M., Maier, H.J., Britton, P., Langereis, M.A., Koumans, J., Wiegertjes, G.F., Forlenza, M., 2015. Activation of the chicken type I interferon response by infectious bronchitis coronavirus. J. Virol. 89, 1156–1167.
La Bonnardiere, C., Laude, H., 1981. High interferon titer in newborn pig intestine during experimentally induced viral enteritis. Infect. Immun. 32, 28–31.
LaMorte, V.J., Dyck, J.A., Ochs, R.L., Evans, R.M., 1998. Localization of nascent RNA and CREB binding protein with the PML-containing nuclear body. Proc. Natl. Acad. Sci. U.S.A. 95, 4991–4996.
Lau, S.K., Lau, C.C., Chan, K.H., Li, C.P., Chen, H., Jin, D.Y., Chan, J.F., Woo, P.C., Yuen, K.Y., 2013. Delayed induction of proinflammatory cytokines and suppression of innate antiviral response by the novel Middle East respiratory syndrome coronavirus: implications for pathogenesis and treatment. J. Gen. Virol. 94, 2679–2690.
Lee, H.M., Lee, B.J., Tae, J.H., Kweon, C.H., Lee, Y.S., Park, J.H., 2000. Detection of porcine epidemic diarrhea virus by immunohistochemistry with recombinant antibody produced in phages. J. Vet. Med. Sci. 62, 333–337.
Lee, S.M., Schommer, S.K., Kleiboeker, S.B., 2004. Porcine reproductive and respiratory syndrome virus field isolates differ in in vitro interferon phenotypes. Vet. Immunol. Immunopathol. 102, 217–231.
Li, B.X., Ge, J.W., Li, Y.J., 2007. Porcine aminopeptidase N is a functional receptor for the PEDV coronavirus. Virology 365, 166–172.
Li, C., Li, Z., Zou, Y., Wicht, O., van Kuppeveld, F.J., Rottier, P.J., Bosch, B.J., 2013. Manipulation of the porcine epidemic diarrhea virus genome using targeted RNA recombination. PLoS One 8, e69997.
Li, J., Liu, Y., Zhang, X., 2010. Murine coronavirus induces type I interferon in oligodendrocytes through recognition by RIG-I and MDA5. J. Virol. 84, 6472–6482.
Li, W., Li, H., Liu, Y., Pan, Y., Deng, F., Song, Y., Tang, X., He, Q., 2012. New variants of porcine epidemic diarrhea virus, China, 2011. Emerg. Infect. Dis. 18, 1350–1353.
Lin, R., Heylbroeck, C., Pitha, P.M., Hiscott, J., 1998. Virus-dependent phosphorylation of the IRF-3 transcription factor regulates nuclear translocation, transactivation potential, and proteasome-mediated degradation. Mol. Cell Biol. 18, 2986–2996.
Livak, K.J., Schmittgen, T.D., 2001. Analysis of relative gene expression data using real-time quantitative PCR and the 2(-Delta Delta C(T)) Method. Methods 25, 402–408.
Lokugamage, K.G., Narayanan, K., Huang, C., Makino, S., 2012. Severe acute respiratory syndrome coronavirus protein nsp1 is a novel eukaryotic translation inhibitor that represses multiple steps of translation initiation. J. Virol. 86, 13598–13608.
Long, J., Wang, G., Matsuura, I., He, D., Liu, F., 2004. Activation of Smad transcriptional activity by protein inhibitor of activated STAT3 (PIAS3). Proc. Natl. Acad. Sci. U.S.A. 101, 99–104.
Marthaler, D., Jiang, Y., Otterson, T., Goyal, S., Rossow, K., Collins, J., 2013. Complete genome sequence of porcine epidemic diarrhea virus strain USA/Colorado/2013 from the United States. Genome Announc. 1, e00555-13.
Melroe, G.T., Silva, L., Schaffer, P.A., Knipe, D.M., 2007. Recruitment of activated IRF-3 and CBP/p300 to herpes simplex virus ICP0 nuclear foci: potential role in blocking IFN-beta induction. Virology 360, 305–321.
Merika, M., Williams, A.J., Chen, G., Collins, T., Thanos, D., 1998. Recruitment of CBP/p300 by the IFN beta enhanceosome is required for synergistic activation of transcription. Mol. Cell 1, 277–287.
Mole, B., 2013. Deadly pig virus slips through US borders. Nature 499, 388.
Nam, E., Lee, C., 2010. Contribution of the porcine aminopeptidase N (CD13) receptor density to porcine epidemic diarrhea virus infection. Vet. Microbiol. 144, 41–50.
Narayanan, K., Huang, C., Lokugamage, K., Kamitani, W., Ikegami, T., Tseng, C.T., Makino, S., 2008. Severe acute respiratory syndrome coronavirus nsp1 suppresses host gene expression, including that of type I interferon, in infected cells. J. Virol. 82, 4471–4479.
Narayanan, K., Ramirez, S.I., Lokugamage, K.G., Makino, S., 2015. Coronavirus nonstructural protein 1: common and distinct functions in the regulation of host and viral gene expression. Virus Res. 202, 89–100.
Overend, C., Mitchell, R., He, D., Rompato, G., Grubman, M.J., Garmendia, A.E., 2007. Recombinant swine beta interferon protects swine alveolar macrophages and MARC-145 cells from infection with Porcine reproductive and respiratory syndrome virus. J. Gen. Virol. 88, 925–931.
Panne, D., Maniatis, T., Harrison, S.C., 2007. An atomic model of the interferon-beta enhanceosome. Cell 129, 1111–1123.
Park, J.E., Cruz, D.J., Shin, H.J., 2011. Receptor-bound porcine epidemic diarrhea virus spike protein cleaved by trypsin induces membrane fusion. Arch. Virol. 156, 1749–1756.
Park, J.E., Shin, H.J., 2014. Porcine epidemic diarrhea virus infects and replicates in porcine alveolar macrophages. Virus Res. 191, 143–152.
Patel, D., Nan, Y., Shen, M., Ritthipichai, K., Zhu, X., Zhang, Y.J., 2010. Porcine reproductive and respiratory syndrome virus inhibits type I interferon signaling by blocking STAT1/STAT2 nuclear translocation. J. Virol. 84, 11045–11055.
Pei, J., Sekellick, M.J., Marcus, P.I., Choi, I.S., Collisson, E.W., 2001. Chicken interferon type I inhibits infectious bronchitis virus replication and associated respiratory illness. J. Interferon Cytokine Res. 21, 1071–1077.
Puranaveja, S., Poolperm, P., Lertwatcharasarakul, P., Kesdaengsakonwut, S., Boonsoongnern, A., Urairong, K., Kitikoon, P., Choojai, P., Kedkovid, R., Teankum, K., Thanawongnuwech, R., 2009. Chinese-like strain of porcine epidemic diarrhea virus, Thailand. Emerg. Infect. Dis. 15, 1112–1115.
Rajsbaum, R., Garcia-Sastre, A., 2013. Viral evasion mechanisms of early antiviral responses involving regulation of ubiquitin pathways. Trends Microbiol. 21, 421–429.
Roth-Cross, J.K., Bender, S.J., Weiss, S.R., 2008. Murine coronavirus mouse hepatitis virus is recognized by MDA5 and induces type I interferon in brain macrophages/microglia. J. Virol. 82, 9829–9838.
Robles, M.T. Saenz, Shivalila, C., Wano, J., Sorrells, S., Roos, A., Pipas, J.M., 2013. Two independent regions of simian virus 40 T antigen increase CBP/p300 levels, alter patterns of cellular histone acetylation, and immortalize primary cells. J. Virol. 87, 13499–13509.
Schwarz, B., Routledge, E., Siddell, S.G., 1990. Murine coronavirus nonstructural protein ns2 is not essential for virus replication in transformed cells. J. Virol. 64, 4784–4791.

Sharma, S., tenOever, B.R., Grandvaux, N., Zhou, G.P., Lin, R., Hiscott, J., 2003. Triggering the interferon antiviral response through an IKK-related pathway. Science 300, 1148–1151.
Shi, C.S., Qi, H.Y., Boularan, C., Huang, N.N., Abu-Asab, M., Shelhamer, J.H., Kehrl, J.H., 2014. SARS-coronavirus open reading frame-9b suppresses innate immunity by targeting mitochondria and the MAVS/TRAF3/TRAF6 signalosome. J. Immunol. 193, 3080–3089.
Siu, K.L., Chan, C.P., Kok, K.H., Chiu-Yat Woo, P., Jin, D.Y., 2014. Suppression of innate antiviral response by severe acute respiratory syndrome coronavirus M protein is mediated through the first transmembrane domain. Cell. Mol. Immunol. 11, 141–149.
Siu, K.L., Kok, K.H., Ng, M.H., Poon, V.K., Yuen, K.Y., Zheng, B.J., Jin, D.Y., 2009. Severe acute respiratory syndrome coronavirus M protein inhibits type I interferon production by impeding the formation of TRAF3.TANK.TBK1/IKKepsilon complex. J. Biol. Chem. 284, 16202–16209.
Song, C., Krell, P., Yoo, D., 2010. Nonstructural protein 1alpha subunit-based inhibition of NF-kappaB activation and suppression of interferon-beta production by porcine reproductive and respiratory syndrome virus. Virology 407, 268–280.
Song, D., Park, B., 2012. Porcine epidemic diarrhoea virus: a comprehensive review of molecular epidemiology, diagnosis, and vaccines. Virus Genes 44, 167–175.
Spiegel, M., Pichlmair, A., Martinez-Sobrido, L., Cros, J., Garcia-Sastre, A., Haller, O., Weber, F., 2005. Inhibition of Beta interferon induction by severe acute respiratory syndrome coronavirus suggests a two-step model for activation of interferon regulatory factor 3. J. Virol. 79, 2079–2086.
St-Germain, J.R., Chen, J., Li, Q., 2008. Involvement of PML nuclear bodies in CBP degradation through the ubiquitin–proteasome pathway. Epigenetics 3, 342–349.
Stark, G.R., Darnell Jr., J.E., 2012. The JAK-STAT pathway at twenty. Immunity 36, 503–514.
Stevenson, G.W., Hoang, H., Schwartz, K.J., Burrough, E.R., Sun, D., Madson, D., Cooper, V.L., Pillatzki, A., Gauger, P., Schmitt, B.J., Koster, L.G., Killian, M.L., Yoon, K.J., 2013. Emergence of Porcine epidemic diarrhea virus in the United States: clinical signs, lesions, and viral genomic sequences. J. Vet. Diagn. Investig. 25, 649–654.
Sueyoshi, M., Tsuda, T., Yamazaki, K., Yoshida, K., Nakazawa, M., Sato, K., Minami, T., Iwashita, K., Watanabe, M., Suzuki, Y., et al., 1995. An immunohistochemical investigation of porcine epidemic diarrhoea. J. Comp. Pathol. 113, 59–67.
Sun, R.Q., Cai, R.J., Chen, Y.Q., Liang, P.S., Chen, D.K., Song, C.X., 2012a. Outbreak of porcine epidemic diarrhea in suckling piglets China. Emerg. Infect. Dis. 18, 161–163.
Sun, Y., Han, M., Kim, C., Calvert, J.G., Yoo, D., 2012b. Interplay between interferon-mediated innate immunity and porcine reproductive and respiratory syndrome virus. Viruses 4, 424–446.
Taguchi, F., Matsuyama, S., 2002. Soluble receptor potentiates receptor-independent infection by murine coronavirus. J. Virol. 76, 950–958.
Tanaka, T., Kamitani, W., DeDiego, M.L., Enjuanes, L., Matsuura, Y., 2012. Severe acute respiratory syndrome coronavirus nsp1 facilitates efficient propagation in cells through a specific translational shutoff of host mRNA. J. Virol. 86, 11128–11137.
Totura, A.L., Baric, R.S., 2012. SARS coronavirus pathogenesis: host innate immune responses and viral antagonism of interferon. Curr. Opin. Virol. 2, 264–275.
Vogt, C., Preuss, E., Mayer, D., Weber, F., Schwemmle, M., Kochs, G., 2008. The interferon antagonist ML protein of thogoto virus targets general transcription factor IIB. J. Virol. 82, 11446–11453.
Wang, K., Lu, W., Chen, J., Xie, S., Shi, H., Hsu, H., Yu, W., Xu, K., Bian, C., Fischer, W.B., Schwarz, W., Feng, L., Sun, B., 2012. PEDV ORF3 encodes an ion channel protein and regulates virus production. FEBS Lett. 586, 384–391.
Wang, Y., Shi, H., Rigolet, P., Wu, N., Zhu, L., Xi, X.G., Vabret, A., Wang, X., Wang, T., 2010. Nsp1 proteins of group I and SARS coronaviruses share structural and functional similarities. Infect. Genet. Evol. 10, 919–924.
Wicht, O., Li, W., Willems, L., Meuleman, T.J., Wubbolts, R.W., van Kuppeveld, F.J., Rottier, P.J., Bosch, B.J., 2014. Proteolytic activation of the porcine epidemic diarrhea coronavirus spike fusion protein by trypsin in cell culture. J. Virol. 88, 7952–7961.
Wood, E.N., 1977. An apparently new syndrome of porcine epidemic diarrhoea. Vet. Rec. 100, 243–244.
Wurm, T., Wright, D.G., Polakowski, N., Mesnard, J.M., Lemasson, I., 2012. The HTLV-1-encoded protein HBZ directly inhibits the acetyl transferase activity of p300/CBP. Nucleic Acids Res. 40, 5910–5925.
Xing, J., Ni, L., Wang, S., Wang, K., Lin, R., Zheng, C., 2013a. Herpes simplex virus 1-encoded tegument protein VP16 abrogates the production of beta interferon (IFN) by inhibiting NF-kappaB activation and blocking IFN regulatory factor 3 to recruit its coactivator CBP. J. Virol. 87, 9788–9801.
Xing, Y., Chen, J., Tu, J., Zhang, B., Chen, X., Shi, H., Baker, S.C., Feng, L., Chen, Z., 2013b. The papain-like protease of porcine epidemic diarrhea virus negatively regulates type I interferon pathway by acting as a viral deubiquitinase. J. Gen. Virol. 94, 1554–1567.
Yang, X., Huo, J.Y., Chen, L., Zheng, F.M., Chang, H.T., Zhao, J., Wang, X.W., Wang, C.Q., 2013. Genetic variation analysis of reemerging porcine epidemic diarrhea virus prevailing in central China from 2010 to 2011. Virus Genes 46, 337–344.
Zhang, J., Yamada, O., Kawagishi, K., Araki, H., Yamaoka, S., Hattori, T., Shimotohno, K., 2008. Human T-cell leukemia virus type 1 Tax modulates interferon-alpha signal transduction through competitive usage of the coactivator CBP/p300. Virology 379, 306–313.
Zhao, L., Jha, B.K., Wu, A., Elliott, R., Ziebuhr, J., Gorbalenya, A.E., Silverman, R.H., Weiss, S.R., 2012. Antagonism of the interferon-induced OAS-RNase L pathway by murine coronavirus ns2 protein is required for virus replication and liver pathology. Cell Host Microbe 11, 607–616.
Zhao, S., Gao, J., Zhu, L., Yang, Q., 2014. Transmissible gastroenteritis virus and porcine epidemic diarrhoea virus infection induces dramatic changes in the tight junctions and microfilaments of polarized IPEC-J2 cells. Virus Res. 192, 34–45.
Zhou, H., Perlman, S., 2007. Mouse hepatitis virus does not induce Beta interferon synthesis and does not inhibit its induction by double-stranded RNA. J. Virol. 81, 568–574.
Zhou, J., Chu, H., Li, C., Wong, B.H., Cheng, Z.S., Poon, V.K., Sun, T., Lau, C.C., Wong, K. K., Chan, J.Y., Chan, J.F., To, K.K., Chan, K.H., Zheng, B.J., Yuen, K.Y., 2014. Active replication of Middle East respiratory syndrome coronavirus and aberrant induction of inflammatory cytokines and chemokines in human macrophages: implications for pathogenesis. J. Infect. Dis. 209, 1331–1342.
Zielecki, F., Weber, M., Eickmann, M., Spiegelberg, L., Zaki, A.M., Matrosovich, M., Becker, S., Weber, F., 2013. Human cell tropism and innate immune system interactions of human respiratory coronavirus EMC compared to those of severe acute respiratory syndrome coronavirus. J. Virol. 87, 5300–5304.